

Statistical studies of Spinning Black-Hole Binaries

Carlos O. Lousto, Hiroyuki Nakano, Yosef Zlochower, Manuela Campanelli

*Center for Computational Relativity and Gravitation,
and School of Mathematical Sciences, Rochester Institute of Technology,
85 Lomb Memorial Drive, Rochester, New York 14623*

We study the statistical distributions of the spins of generic black-hole binaries during the inspiral and merger, as well as the distributions of the remnant mass, spin, and recoil velocity. For the inspiral regime, we start with a random uniform distribution of spin directions \vec{S}_1 and \vec{S}_2 over the sphere and magnitudes $|\vec{S}_1/m_1^2| = |\vec{S}_2/m_2^2| = 0.97$ for different mass ratios. Starting from a fiducial initial separation of $r_i = 50m$, we perform 3.5-post-Newtonian-order evolutions down to a separation of $r_f = 5m$, where $m = m_1 + m_2$, the total mass of the system. At this final fiducial separation, we compute the angular distribution of the spins with respect to the final orbital angular momentum, \vec{L} . We perform $16^4 = 65536$ simulations for six mass ratios between $q = 1$ and $q = 1/16$ and compute the distribution of the angles $\hat{\vec{L}} \cdot \hat{\vec{S}}$ and $\hat{\vec{L}} \cdot \hat{\vec{S}}$, directly related to recoil velocities and total angular momentum. We find a small but statistically significant bias of the distribution towards counter-alignment of both scalar products. A post-Newtonian analysis shows that radiation-reaction-driven dissipative effects on the orbital angular momentum lead to this bias. To study the merger of black-hole binaries, we turn to full numerical techniques. In order to make use of the numerous simulations now available in the literature, we introduce empirical formulae to describe the final remnant black hole mass, spin, and recoil velocity for merging black-hole binaries with arbitrary mass ratios and spins. Our formulae are based on the post-Newtonian scaling, to model the plunge phase, with amplitude parameters chosen by a least-squares fit of recently available fully nonlinear numerical simulations, supplemented by inspiral losses from infinity to the ISCO. We then evaluate those formulae for randomly chosen directions of the individual spins and magnitudes as well as the binary's mass ratio. The number of evaluations has been chosen such that there are 10 configurations per each dimension of this parameter space, i.e. 10^7 . We found that the magnitude of the recoil velocity distribution decays exponentially as $P(v) \sim \exp(-v/2500 \text{ km s}^{-1})$ with mean velocity $\langle v \rangle = 630 \text{ km s}^{-1}$ and standard deviation $\sqrt{\langle v^2 \rangle - \langle v \rangle^2} = 534 \text{ km s}^{-1}$, leading to a 23% probability of recoils larger than 1000 km s^{-1} , and a highly peaked angular distribution along the final orbital axis. The studies of the distribution of the final black-hole spin magnitude show a universal distribution highly peaked at $S_f/m_f^2 = 0.73$ and a 25° misalignment with respect to the final orbital angular momentum, just prior to full merger of the holes. We also compute the statistical dependence of the magnitude of the recoil velocity with respect to the ejection angle. The spin and recoil velocity distributions are also displayed as a function of the mass ratio. We finally also compute the effects of the observer orientation with respect to the recoil velocity vector to take into account the probabilities to measure a given redshifted (or blueshifted) radial velocity of accretion disks with respect to host galaxies.

PACS numbers: 04.25.Dm, 04.25.Nx, 04.30.Db, 04.70.Bw

I. INTRODUCTION

The relevance of the spins to the dynamics of black-hole (BH) mergers was recognized soon after the breakthrough in numerical relativity [1, 2, 3] that allowed for the long term, stable numerical evolution of such systems. Notable examples of the early findings are the ‘hangup’ effect [4], a repulsive spin-orbit interaction, that delays the merger of black-hole binaries (BHB) when the spins are aligned with the orbital angular momentum, and simultaneously causes the system to radiate excess angular momentum, leading to a remnant BH with sub-maximal spin. The same mechanism produces an additional attractive effect when the spins are counter-aligned with the orbital angular momentum, leading to a prompt merger. Thus the radiation of angular momentum and energy is asymmetric with respect to the relative orien-

tations of the total spin $\vec{S} = \vec{S}_1 + \vec{S}_2$ and the orbital angular momentum \vec{L} .

When the spins are not exactly aligned or counter aligned, new effects appear (the hangup effect is still present). Precession of the spins is important dynamically because it cause the orbital plane to strongly precess just prior to merger [5]. The final spin of the merged hole can flip with respect to the directions of the individual ones, mainly due to the addition of the orbital angular momentum [5]. While the spin-orbit coupling leads to strong precessional effects near merger, the magnitudes of the spins are not affected to the same degree. In particular spin-orbit interactions are too weak to induce the binary to corotate (or maintain corotation of an initially corotating binary) at the last stages of the merger because the timescale for the radiation driven inspiral is much smaller than the spin-orbit interaction

timescale [6].

Numerous other papers have studied different spin effects, such as the large recoil velocities acquired by the remnant of the merger of two spinning black holes [7, 8, 9, 10, 11, 12] and long term evolutions of generic BHBs (i.e. unequal mass and unequal, randomly-oriented spins) [13, 14] to cite a few of the nearly one hundred papers published on the subject since 2006.

The characterization of the remnant black hole (BH) as the by-product of a generic BH binary (BHB) merger is of great astrophysical interest as it allows one to model the growth of BHs during the evolution of the universe and their effect on the dynamical evolution of galactic cores and globular clusters, as well as the collisions of galaxies and stellar size binary systems. Thanks to the recent breakthroughs in Numerical Relativity [1, 2, 3] one can now precisely compute the masses, spins and recoil velocities of these merged BHBs from fully nonlinear numerical simulations.

The modeling of the remnant black hole using fully-numerical techniques was pioneered by the ‘Lazarus method’ [15] for spinning black holes followed by the breakthrough ‘moving puncture’ approach. In Refs. [4, 5, 6] the authors studied BHBs characterized by equal-mass, equal-spin individual BHs, with the spins aligned or counter-aligned with the orbital angular momentum, using fully nonlinear numerical calculations and found a simple *ad hoc* expression relating the final mass and spin of the remnant with the spins of the individual BHs. This scenario was later revisited in [16, 17] and the formula for the remnant spin was generalized (by assuming that the angular momentum is only radiated along the orbital axis, and neglecting the energy loss) in [18] for arbitrary BH configurations (although in the latest paper of this sequel this condition was removed [19].) In [20] a more general *ad hoc* fitting function was proposed. A more comprehensive approach was proposed in [21]; where a generic Taylor expansion, reduced by the physical symmetries of the problem, was used to fit the existing full numerical simulations. A different approach was presented in [22] where the particle limit approximation was extended to the equal-mass case and the effects of post-ISCO (Innermost Stable Circular Orbit) gravitational radiation were neglected. This approach was further improved in [23] by taking binding energies into account. All of these approaches show a certain degree of agreement with the remnant masses and spins obtained in the few dozen fully nonlinear numerical simulations available, but there remains significant uncertainties concerning their accuracy outside this range of parameters. In this paper we propose a set of formulae that incorporate the benefits of both approaches in a unified way.

Due to the large astrophysical interest of computing remnant recoil velocities, the modeling of recoil velocities followed an independent path, particularly since the discovery [7, 24] that the spins of the black holes play a crucial role in producing recoils of up to 4000 km s^{-1} . The importance of modeling the recoil velocities as a function

of the astrophysical parameters of the progenitor binary was quickly realized [7, 8, 24].

The news that the merger of binary black holes can produce recoil velocities up to 4000 km s^{-1} , and hence allow the remnant to escape from major galaxies, led to numerous theoretical and observational efforts to find traces of this phenomenon. Several studies made predictions of specific observational features of recoiling super-massive black holes in the cores of galaxies in the electromagnetic spectrum [25, 26, 27, 28, 29, 30, 31] from infrared [32] to X-rays [33, 34, 35] and morphological aspects of the galaxy cores [36, 37, 38]. Notably, there began to appear observations indicating the possibility of detection of such effects [39, 40, 41], and although alternative explanations are possible [42, 43, 44, 45], there is still the exciting possibility that these observations can lead to the first confirmation of a prediction of General Relativity in the highly-dynamical, strong-field regime.

In our approach to the recoil problem [7, 24] we chose to use post-Newtonian theory as a guide to model the recoil dependence on the physical parameters of the progenitor BHB (See Eqs. (3.31) in [46]), while arguing that only full numerical simulations can produce the correct amplitude of the effect. Bearing this in mind, we proposed an empirical formula for the total recoil velocities (see Eq. (22) below.) Our heuristic formula describing the recoil velocity of a black-hole binary remnant as a function of the parameters of the individual holes has been theoretically verified in several ways. In [24] the $\cos \Theta$ dependence was established and was confirmed in [47] for binaries with different initial separations. In [48] the decomposition into spin components perpendicular and parallel to the orbital plane was verified, and in [49] it was found that the quadratic-in-spin corrections to the in-plane recoil velocity are less than 20 km s^{-1} . Recently in [50] we confirmed the leading η^2 (where η is the symmetric mass ratio) dependence of the large recoils out of the orbital plane.

Since the magnitude (and direction) of the recoil velocity of the remnant black holes depend so sensitively on the spin orientation just around the time of the formation of a common event horizon, it is important to establish that random oriented spins of individual black holes at large separations (as a plausible initial astrophysical scenario) lead to randomly oriented black holes near merger, or if there is some bias in their orientations by the time they get very close together (i.e. at typical numerical simulations separations of a few M). It has been argued recently [51, 52, 53] that the presence of gas and accretion of the individual black holes during the inspiral phase for long time scales can lead to a preferential alignment of spins with the orbital angular momentum, and hence to a configuration that leads to modest recoil velocities (a few hundred km s^{-1}). While the verification of this claim for ‘wet’ mergers is underway, in this paper we would like to explore the possibility that such alignment (or counter-alignment) mechanism exists for purely gravitational interactions (‘dry mergers’). In general we will

seek to find if there is any bias in the individual spin distributions of black holes at close separations ($5 - 8M$ for starting typical full numerical evolutions) when starting evolutions with post-Newtonian methods at large radii with random spin orientations. These distributions, in turn, will then help in choosing configuration for full numerical simulations of close binaries.

The paper is organized as follows. In Section II we describe the post-Newtonian formalism to analyze the inspiral stage of the binary evolutions. We use the Hamiltonian formulation (up to 3.5PN order) to derive the equations of motion in the ADM-TT gauge. Conservative and radiative effects of the spins are included up to the next leading PN order. We also include a purely analytic analysis of the projection of the quantity $\vec{\Delta}$ along the orbital angular momentum \vec{L} , which has a strong effect on the recoil velocity, to qualitatively predict a slight bias towards counter-alignment of these two vectors. The results of the statistics of numerical integration of the post-Newtonian equations of motion (EOM) follows. We performed integrations from initial separations of $r = 50M$ with 16^4 spin orientation chosen at random and magnitudes fixed at large astrophysical values, i.e. $S_i/m_i^2 = 0.97$ for different mass ratios in the range $1/16 \leq q = m_1/m_2 \leq 1$. The results quantitatively confirm the bias towards counter-alignment of $\vec{\Delta}$ and total spin \vec{S} with respect to the orbital angular momentum \vec{L} . Section III deals with the merger phase, when the black holes are much closer to each other and in a few orbits will merge into a single larger one. This is the typical scenario that full numerical simulations assume. The bulk properties of the remnant black hole can be summarized in terms of empirical remnant formulae that describe its total mass, spin and recoil velocity. We proposed formulae for these quantities based on post-Newtonian scaling with amplitudes fixed by the full numerical simulations. With these formulae at hand, we perform statistical studies by evaluation of these expression for random distributions of mass ratios and individual spins (magnitudes and spins). Those evaluations lead to a large recoil velocity tail in the distribution with non negligible probabilities for $v > 1000 \text{ km s}^{-1}$, and highly peaked about the direction of orbital angular momentum at merger. Likewise, evaluations of the final spin formulae lead to a wide distribution peaked at magnitudes of $S_f/M_f^2 \approx 0.73$ and orientations peaked at an angle $\sim 25^\circ$ with respect to the orbital angular momentum. We complete the paper with a discussion of the astrophysical consequences of these results and include an appendix with the computation of the innermost stable circular orbit radius, energy and angular momentum around Kerr black holes (needed for the remnant formulae), with an analytic solution for the equatorial and polar orbits.

II. INSPIRAL PHASE OF BHBS

A. PN techniques

We construct the PN equations of motion using the formulae provided in Refs. [54, 55, 56, 57]. To obtain the conservative part of the PN equations of motion, we use the following Hamiltonian,

$$\begin{aligned} H = & H_{\text{O,Newt}} + H_{\text{O,1PN}} + H_{\text{SO,1.5PN}} + H_{\text{O,2PN}} \\ & + H_{\text{SS,2PN}} + H_{\text{SO,2.5PN}} + H_{\text{O,3PN}} \\ & + H_{\text{S}_1\text{S}_2,3\text{PN}} + H_{\text{S}_1\text{S}_1(\text{S}_2\text{S}_2),3\text{PN}}, \end{aligned} \quad (1)$$

where H_{O} contains the terms associated with the orbital motion up to 3PN order, H_{SO} contains the spin-orbit coupling terms up to 2.5PN order, and H_{SS} contains the spin-spin coupling term up to 3PN order. Note that Porto and Rothstein has discussed the spin-spin interaction by using effective field theory techniques [58, 59, 60, 61]. These are a very powerful approach to systematically discuss the dynamics of finite size objects.

The equations of motion are then obtained via,

$$\frac{dX^i}{dt} = \{X^i, H\} = \frac{\partial H}{\partial P_i}, \quad (2)$$

$$\frac{dP_i}{dt} = \{P_i, H\} + F_i = -\frac{\partial H}{\partial X^i} + F_i, \quad (3)$$

$$\frac{d\vec{S}_1}{dt} = \{\vec{S}_1, H\} = \frac{\partial H}{\partial \vec{S}_1} \times \vec{S}_1, \quad (4)$$

$$\frac{d\vec{S}_2}{dt} = \{\vec{S}_2, H\} = \frac{\partial H}{\partial \vec{S}_2} \times \vec{S}_2, \quad (5)$$

where $\{\dots, \dots\}$ denotes the Poisson brackets, $X^i = x_1^i - x_2^i$ and P^i are relative coordinates and linear momenta of the binary, \vec{S}_1 and \vec{S}_2 are the spins of each body, and F_i is the radiation reaction force. The radiation reaction force \vec{F} is given by [54],

$$\begin{aligned} \vec{F} = & \frac{1}{\omega |\vec{L}|} \frac{dE}{dt} \vec{P} \\ & + \frac{8}{15} \eta^2 \frac{v_\omega^8}{|\vec{L}|^2 R} \left\{ \left(61 + 48 \frac{m_2}{m_1} \right) \vec{P} \cdot \vec{S}_1 \right. \\ & \left. + \left(61 + 48 \frac{m_1}{m_2} \right) \vec{P} \cdot \vec{S}_2 \right\} \vec{L}, \end{aligned} \quad (6)$$

where $\vec{L} = \vec{X} \times \vec{P}$, $R = |\vec{X}|$, $v_\omega = (M\omega)^{1/3}$ and ω is the

orbital frequency. We use the following notation:

$$M = m_1 + m_2, \quad (7)$$

$$\delta m = m_1 - m_2, \quad (8)$$

$$\eta = \frac{m_1 m_2}{M^2}, \quad (9)$$

$$\vec{S} = \vec{S}_1 + \vec{S}_2, \quad (10)$$

$$\vec{\Delta} = M \left(\frac{\vec{S}_2}{m_2} - \frac{\vec{S}_1}{m_1} \right), \quad (11)$$

$$\begin{aligned} \vec{S}_0 &= 2\vec{S} + \frac{\delta m}{M} \vec{\Delta} \\ &= \left(1 + \frac{m_2}{m_1}\right) \vec{S}_1 + \left(1 + \frac{m_1}{m_2}\right) \vec{S}_2. \end{aligned} \quad (12)$$

To calculate dE/dt , the instantaneous loss in energy, we use the formulae given in Refs. [62] [102].

1. PN prediction of distribution of $\hat{\vec{L}} \cdot \hat{\vec{\Delta}}$

The time derivative of the inner product $\hat{\vec{L}} \cdot \hat{\vec{\Delta}}$ where $\hat{\vec{L}}$ and $\hat{\vec{\Delta}}$ are the unit vector corresponding to \vec{L} and $\vec{\Delta}$, respectively, is given by

$$\begin{aligned} (\hat{\vec{L}} \cdot \hat{\vec{\Delta}})^\cdot &= \frac{\dot{\vec{L}} \cdot \vec{\Delta}}{|\vec{L}||\vec{\Delta}|} + \frac{\vec{L} \cdot \dot{\vec{\Delta}}}{|\vec{L}||\vec{\Delta}|} \\ &\quad - \frac{\vec{L} \cdot \vec{\Delta} |\dot{\vec{L}}|}{|\vec{L}|^2 |\vec{\Delta}|} - \frac{\vec{L} \cdot \vec{\Delta} |\dot{\vec{\Delta}}|}{|\vec{L}||\vec{\Delta}|^2}. \end{aligned} \quad (13)$$

Here since we focus only on the dissipative effect, we ignore $\dot{\vec{\Delta}}$ and $|\dot{\vec{\Delta}}|$. This is because there is no radiation reaction term in Eqs. (4) and (5). The radiation reaction effect are introduced by the evolution equation of the linear momentum given in Eq. (3). Furthermore, we expect that the time evolution of the spin directions due to the conservative force will cancel out in a statistical treatment. Hence, we have

$$(\hat{\vec{L}} \cdot \hat{\vec{\Delta}})^\cdot_{\text{dis}} = \frac{\dot{\vec{L}}_{\text{dis}} \cdot \vec{\Delta}}{|\vec{L}||\vec{\Delta}|} - \frac{\vec{L} \cdot \vec{\Delta} |\dot{\vec{L}}|_{\text{dis}}}{|\vec{L}|^2 |\vec{\Delta}|}. \quad (14)$$

The dissipative effect on the angular momentum is given by

$$\begin{aligned} \dot{\vec{L}}_{\text{dis}} &= \vec{X} \times \vec{F} \\ &= \frac{1}{\omega} \frac{dE}{dt} \hat{\vec{L}} \\ &\quad - \frac{8}{15} \eta^2 \frac{v_\omega^8 R}{|\vec{L}|^2} \left\{ \left(61 + 48 \frac{m_2}{m_1}\right) \vec{P} \cdot \vec{S}_1 \right. \\ &\quad \left. + \left(61 + 48 \frac{m_1}{m_2}\right) \vec{P} \cdot \vec{S}_2 \right\} \vec{P} \end{aligned} \quad (15)$$

where we have used the quasi-circular assumption and Eq. (6).

Using this dissipation of the angular momentum, we obtain

$$\begin{aligned} (\hat{\vec{L}} \cdot \hat{\vec{\Delta}})^\cdot_{\text{dis}} &= -\frac{8}{15} \frac{v_\omega^{11}}{M} \frac{q}{(1+q)^4} \frac{1}{|\vec{\alpha}_2 - q\vec{\alpha}_1|} \left\{ -q^2 (61q + 48) (\hat{\vec{P}} \cdot \vec{\alpha}_1)^2 + (61 + 48q) (\hat{\vec{P}} \cdot \vec{\alpha}_2)^2 \right. \\ &\quad \left. + q [(61q + 48) - (61 + 48q)] (\hat{\vec{P}} \cdot \vec{\alpha}_1)(\hat{\vec{P}} \cdot \vec{\alpha}_2) \right\}, \end{aligned} \quad (16)$$

in the leading PN order calculation. Here $\vec{\alpha}_1 = \vec{S}_1/m_1^2$, $\vec{\alpha}_2 = \vec{S}_2/m_2^2$ and $q = m_1/m_2$. Note that the dE/dt term

in $\dot{\vec{L}}_{\text{dis}}$ cancels out, and we have

$$\begin{aligned} (\hat{\vec{L}} \cdot \hat{\vec{S}})^\cdot_{\text{dis}} &= -\frac{8}{15} \frac{v_\omega^{11}}{M} \frac{q}{(1+q)^4} \frac{1}{|q^2 \vec{\alpha}_1 + \vec{\alpha}_2|} \left\{ q^3 (61q + 48) (\hat{\vec{P}} \cdot \vec{\alpha}_1)^2 + (61 + 48q) (\hat{\vec{P}} \cdot \vec{\alpha}_2)^2 \right. \\ &\quad \left. + q [(61q + 48) + q (61 + 48q)] (\hat{\vec{P}} \cdot \vec{\alpha}_1)(\hat{\vec{P}} \cdot \vec{\alpha}_2) \right\}, \end{aligned} \quad (17)$$

Next, we consider the time integration from $t = t_i$ to $t = t_f$.

$$\begin{aligned}
\int_{t_i}^{t_f} (\hat{\vec{L}} \cdot \hat{\vec{\Delta}})_{\text{dis}} dt &= -\frac{5}{64} \frac{(1+q)^2}{q} \int_{R_i}^{R_f} (\hat{\vec{L}} \cdot \hat{\vec{\Delta}})_{\text{dis}} \left(\frac{M}{R}\right)^{-3} dR \\
&= -\frac{1}{36} \frac{1}{(1+q)^2} \frac{1}{|\vec{\alpha}_2 - q\vec{\alpha}_1|} \left\{ -q^2 (61q + 48) (\hat{\vec{P}} \cdot \vec{\alpha}_1)^2 + (61 + 48q) (\hat{\vec{P}} \cdot \vec{\alpha}_2)^2 \right. \\
&\quad \left. + q [(61q + 48) - (61 + 48q)] (\hat{\vec{P}} \cdot \vec{\alpha}_1)(\hat{\vec{P}} \cdot \vec{\alpha}_2) \right\} \left[\left(\frac{M}{R_f}\right)^{3/2} - \left(\frac{M}{R_i}\right)^{3/2} \right], \\
\int_{t_i}^{t_f} (\hat{\vec{L}} \cdot \hat{\vec{S}})_{\text{dis}} dt &= -\frac{5}{64} \frac{(1+q)^2}{q} \int_{R_i}^{R_f} (\hat{\vec{L}} \cdot \hat{\vec{S}})_{\text{dis}} \left(\frac{M}{R}\right)^{-3} dR \\
&= -\frac{1}{36} \frac{1}{(1+q)^2} \frac{1}{|q^2\vec{\alpha}_1 + \vec{\alpha}_2|} \left\{ q^3 (61q + 48) (\hat{\vec{P}} \cdot \vec{\alpha}_1)^2 + (61 + 48q) (\hat{\vec{P}} \cdot \vec{\alpha}_2)^2 \right. \\
&\quad \left. + q [(61q + 48) + q(61 + 48q)] (\hat{\vec{P}} \cdot \vec{\alpha}_1)(\hat{\vec{P}} \cdot \vec{\alpha}_2) \right\} \left[\left(\frac{M}{R_f}\right)^{3/2} - \left(\frac{M}{R_i}\right)^{3/2} \right], \quad (18)
\end{aligned}$$

where we considered only the evolution of v_ω , i.e., the inspiral, and have used the leading radiation reaction and the Newtonian velocity,

$$\begin{aligned}
\frac{dR}{dt} &= -\frac{64}{5} \frac{q}{(1+q)^2} \left(\frac{M}{R}\right)^3, \\
v_\omega &= \sqrt{\frac{M}{R}}. \quad (19)
\end{aligned}$$

In the above integration, we derived the formula assuming $\hat{\vec{P}} \cdot \vec{\alpha}_i = \text{constant}$ ($i = 1, 2$). However, since the spins precess, we need to check the evolution of $\hat{\vec{P}} \cdot \vec{\alpha}_i$. From the evolution equations for spins in the leading PN order, the evolution equations for $\hat{\vec{P}} \cdot \vec{\alpha}_i$ are given by

$$\begin{aligned}
(\hat{\vec{P}} \cdot \vec{\alpha}_1)^\cdot &= \left[-\frac{v_\omega}{R} + \frac{Mv_\omega}{R^2} \frac{1}{(1+q)^2} \left(2q + \frac{3}{2}\right) \right] \\
&\quad \times (\hat{\vec{X}} \cdot \vec{\alpha}_1), \\
(\hat{\vec{P}} \cdot \vec{\alpha}_2)^\cdot &= \left[-\frac{v_\omega}{R} + \frac{Mv_\omega}{R^2} \frac{q}{(1+q)^2} \left(2 + \frac{3}{2}q\right) \right] \\
&\quad \times (\hat{\vec{X}} \cdot \vec{\alpha}_2), \quad (20)
\end{aligned}$$

We note that in the limit $q \rightarrow 0$, we only need to consider the evolution of $\hat{\vec{P}} \cdot \vec{\alpha}_2$ in Eq. (16),

$$(\hat{\vec{P}} \cdot \vec{\alpha}_2)^\cdot = -\frac{v_\omega}{R} (\hat{\vec{X}} \cdot \vec{\alpha}_2). \quad (21)$$

This equation means that the direction of $\vec{\alpha}_2$ does not change, i.e., there is no precession of the spin. Therefore, we may replace $(\hat{\vec{P}} \cdot \vec{\alpha}_2)^2$ in Eq. (18) by the one-orbit average $\langle (\hat{\vec{P}} \cdot \vec{\alpha}_2)^2 \rangle_t$ of $(\hat{\vec{P}} \cdot \vec{\alpha}_2)^2$. Although the adiabatic evolution of $\langle (\hat{\vec{P}} \cdot \vec{\alpha}_2)^2 \rangle_t$ is present, its effect comes in at higher PN order in Eq. (18). In this case, it should

TABLE I: The q dependence in the evolution of $(\hat{\vec{L}} \cdot \hat{\vec{\Delta}})_{\text{dis}}$ and $(\hat{\vec{L}} \cdot \hat{\vec{S}})_{\text{dis}}$ from $r = 50M$ to $r = 5M$. We set $|\vec{\alpha}_1| = |\vec{\alpha}_2| = 0.97$.

q	$(\hat{\vec{L}} \cdot \hat{\vec{\Delta}})_{\text{dis}}$	$(\hat{\vec{L}} \cdot \hat{\vec{S}})_{\text{dis}}$
1.00	0.0000	-0.0283
0.75	-0.0111	-0.0287
0.50	-0.0224	-0.0310
0.25	-0.0343	-0.0366
0.125	-0.0406	-0.0412
0.0625	-0.0440	-0.0441
0.00	-0.0475	-0.0475

be noted that we may consider a test particle orbiting around a Kerr black hole with the spin \vec{S}_2 . According to [63] in the black hole perturbation approach, the particle's angular momentum and the black hole's spin tend to be anti-parallel.

On the other hand, in the case of comparable mass binaries, the direction of $\vec{\alpha}_i$ changes on a timescale much shorter than the integration time. Hence, Eq. (18) is not expected to be accurate in $q \rightarrow 1$ limit.

In Table I, we show the q dependence of Eq. (18) when we ignore the spin precession. Here, we take the average with respect to the direction of two spins to represent the randomly oriented spins. We also present the spin amplitude dependence in Table II.

B. Statistical Results

For our PN evolutions with used an adaptive fourth-order Runge-Kutta time-integration scheme with a relative tolerance of 10^{-13} . The initial data for the simulations were generated using the 3PN conservative equations for quasi-circular orbits with orbital frequency $M\Omega = 0.00275$, which corresponds to an orbital radius

TABLE II: The amplitude dependence of the spin in the evolution of $(\hat{\vec{L}} \cdot \hat{\vec{\Delta}})_{\text{dis}}$ and $(\hat{\vec{L}} \cdot \hat{\vec{S}})_{\text{dis}}$ from $r = 50M$ to $r = 5M$. We set $q = 0.25$ and $|\vec{\alpha}_1| = |\vec{\alpha}_2| = \alpha$.

α	$(\hat{\vec{L}} \cdot \hat{\vec{\Delta}})_{\text{dis}}$	$(\hat{\vec{L}} \cdot \hat{\vec{S}})_{\text{dis}}$
0.97	-0.0343	-0.0366
$0.97/\sqrt{2}$	-0.0242	-0.0259
$0.97/2$	-0.0171	-0.0183
$0.97/4$	-0.0086	-0.0092
$0.97/8$	-0.0043	-0.0046
$0.97/16$	-0.0021	-0.0023

of $50 \pm 2M$. In most cases we stopped the PN simulations at a fixed orbital radius of $5M$, but also performed a set of simulations that terminated at $r = 8M$ in order to see the effect of the final orbital radius on the distributions. To obtain the initial PN orbital parameters, we used uniform distributions of $\vec{\alpha}_1$ and $\vec{\alpha}_2$ over the sphere (by choosing uniform random distributions in $\mu = \cos \theta$ and ϕ) with fix amplitude $\alpha = 0.97$. We produced 65536 random spin configurations for each fix mass ratio $q = 1, 3/4, 1/2, 1/4, 1/8, 1/16$. Each run took approximately 10 minutes. In addition we performed sets of 65536 run for $q = 1/4$ and $\alpha = 0.97/\sqrt{2}$, $\alpha = 0.97/2$, as well as $\alpha = 0.97/\sqrt{2}$ but terminating at $r = 8M$ rather than $r = 5M$. We denote these three latter distributions in Table III by 0.25S1, 0.25S2, and 0.25F, respectively.

In the following section we examine the distribution of the angle $\mu = \hat{\vec{L}} \cdot \hat{\vec{\Delta}}$ that $\vec{\Delta} = M(\vec{S}_2/m_2 - \vec{S}_1/m_1)$ makes with the orbital angular momentum (at $r = 5M$). At $r = 50M$ this distribution is uniform (since \vec{S}_1 and \vec{S}_2 are chosen from a uniform distribution on the sphere). In Figs. 1-6, we show histograms of the distribution of the angle $\hat{\vec{L}} \cdot \hat{\vec{\Delta}}$ that $\vec{\Delta}$ makes with the orbital angular momentum for the given mass ratios. To analyze these data quantitatively, we bin the data from $\mu = -1$ to $\mu = 1$ with bin widths of $\delta\mu = 0.01$. We fit the resulting data $P(\mu)$ to a linear function $P(\mu) = P(0) + \frac{dP}{d\mu}|_0\mu$ for each mass ratio. The results are summarized in Table III and plots of the fits are given in Figs. 9-14. We perform a similar analysis for the angle that \vec{S} makes with the orbital angular momentum (see Fig. 17). We also perform a similar analysis, but with q fixed to $q = 1/4$ and $\alpha_1 = \alpha_2 = \alpha$ reduced by factors of $\sqrt{2}$ and 2, respectively (See Figs. 7-8 and 15-16), and fit the resulting slope $dP/d\mu$ as a function of α . Here the fit favors a leading-order linear dependence in α over a leading-order quadratic dependence (where the constant term is assumed to be zero) (See Fig. 18). If we set the constant in the fit to zero, then a linear dependence is $dP/d\mu = -(0.02491 \pm 0.00098)\alpha$ for the distribution of $\hat{\vec{L}} \cdot \hat{\vec{\Delta}}$ and $dP/d\mu = -(0.0301 \pm 0.0041)\alpha$ for the distribution of the $\hat{\vec{L}} \cdot \hat{\vec{S}}$. Note that the skewing of the distributions takes place at smaller radii, as can be seen by differences in the 0.25S1 and 0.25F distributions, which differ only in the orbital radius ($5M$ for 0.25S1 and

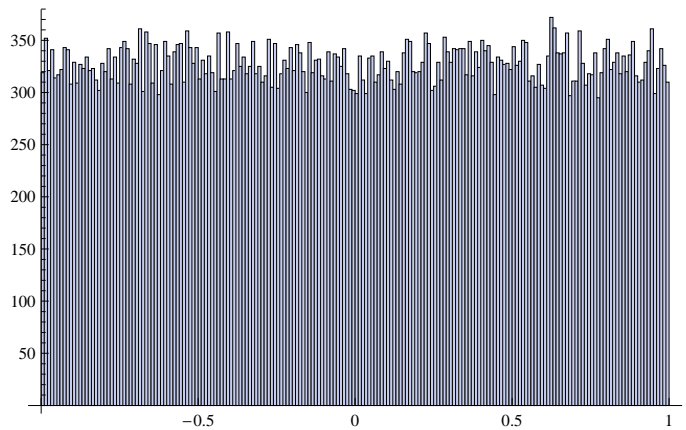


FIG. 1: The $P(\mu = \hat{\vec{L}} \cdot \hat{\vec{\Delta}})$ distribution for $q = 1$ at $r = 5M$ starting from a uniform distribution at $r = 50M$. Here we plot the number of events in the given range of μ out of 16^4 total events.

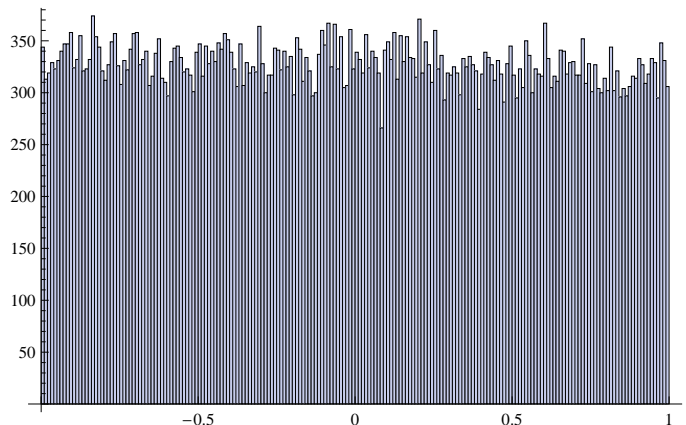


FIG. 2: The $P(\mu = \hat{\vec{L}} \cdot \hat{\vec{\Delta}})$ distribution for $q = 3/4$ at $r = 5M$ starting from a uniform distribution at $r = 50M$. Here we plot the number of events in the given range of μ out of 16^4 total events.

$8M$ for 0.25F) where the distributions are measured. In Table IV we show fits for the distributions of the angles $\hat{S}_1 \cdot \hat{L}$ and $\hat{S}_2 \cdot \hat{L}$ for the same set of runs. Note that the distribution of $\hat{S}_1 \cdot \hat{L}$ (the smaller BH's spin) become essentially uniform for $q < 1/4$.

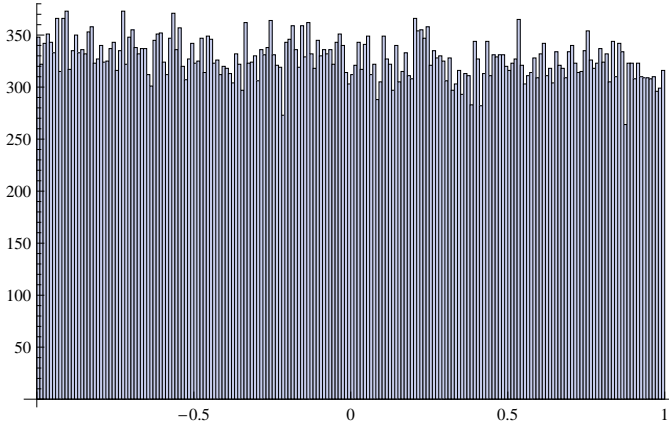


FIG. 3: The $P(\mu = \hat{\vec{L}} \cdot \hat{\vec{\Delta}})$ distribution for $q = 1/2$ at $r = 5M$ starting from a uniform distribution at $r = 50M$. Here we plot the number of events in the given range of μ out of 16^4 total events.

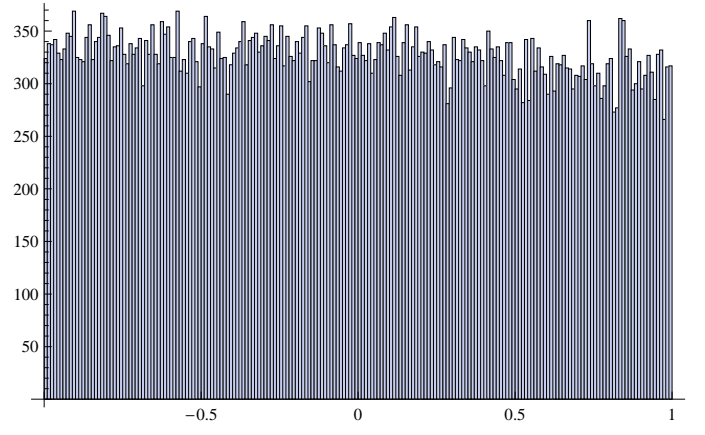


FIG. 6: The $P(\mu = \hat{\vec{L}} \cdot \hat{\vec{\Delta}})$ distribution for $q = 1/16$ at $r = 5M$ starting from a uniform distribution at $r = 50M$. Here we plot the number of events in the given range of μ out of 16^4 total events.

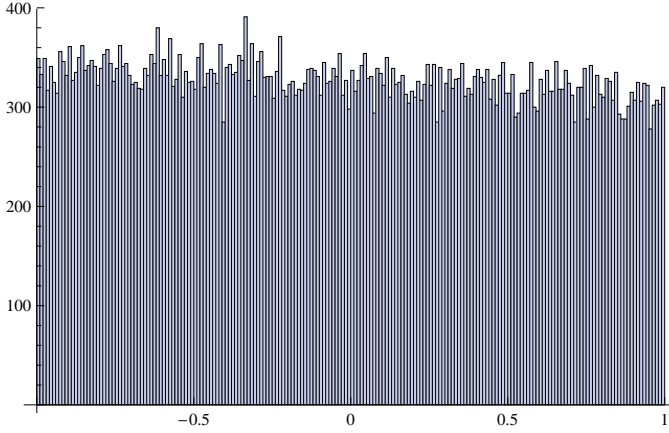


FIG. 4: The $P(\mu = \hat{\vec{L}} \cdot \hat{\vec{\Delta}})$ distribution for $q = 1/4$ at $r = 5M$ starting from a uniform distribution at $r = 50M$. Here we plot the number of events in the given range of μ out of 16^4 total events.

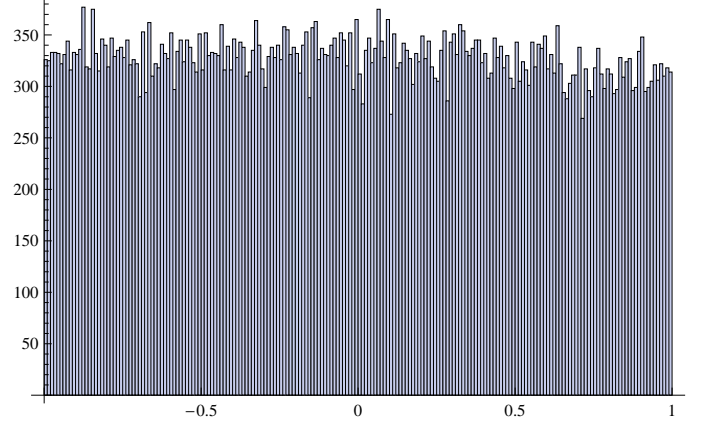


FIG. 7: The $P(\mu = \hat{\vec{L}} \cdot \hat{\vec{\Delta}})$ distribution for $q = 1/4$ at $r = 5M$ starting from a uniform distribution at $r = 50M$ and $\alpha_1 = \alpha_2 = 0.97/\sqrt{2}$. Here we plot the number of events in the given range of μ out of 16^4 total events.

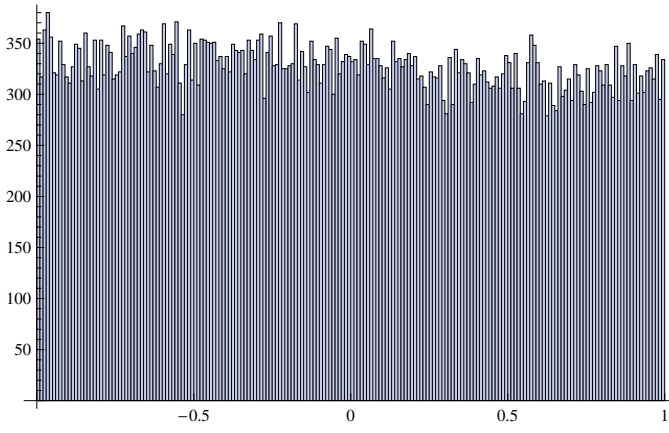


FIG. 5: The $P(\mu = \hat{\vec{L}} \cdot \hat{\vec{\Delta}})$ distribution for $q = 1/8$ at $r = 5M$ starting from a uniform distribution at $r = 50M$. Here we plot the number of events in the given range of μ out of 16^4 total events.

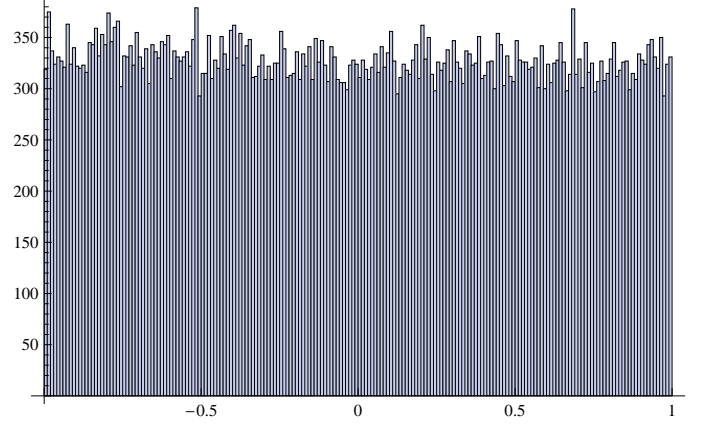


FIG. 8: The $P(\mu = \hat{\vec{L}} \cdot \hat{\vec{\Delta}})$ distribution for $q = 1/4$ at $r = 5M$ starting from a uniform distribution at $r = 50M$ and $\alpha_1 = \alpha_2 = 0.97/2$. Here we plot the number of events in the given range of μ out of 16^4 total events.

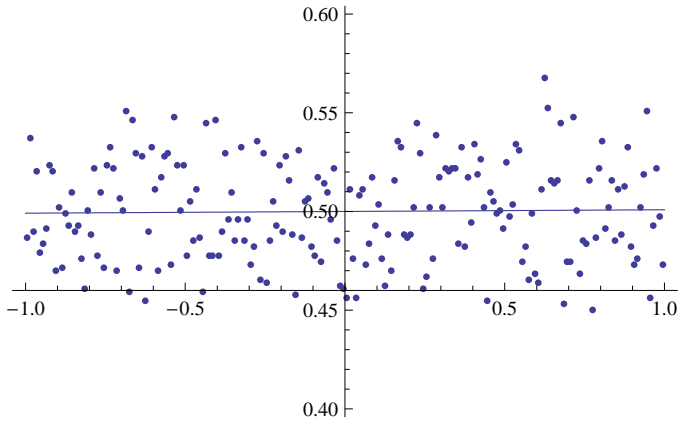


FIG. 9: The fit to the normalized $P(\mu = \hat{L} \cdot \hat{\Delta})$ distribution at $r = 5M$ for $q = 1$. The data have been binned with a bin width of $\delta\mu = 0.01$ and normalized to a total probability of 1.

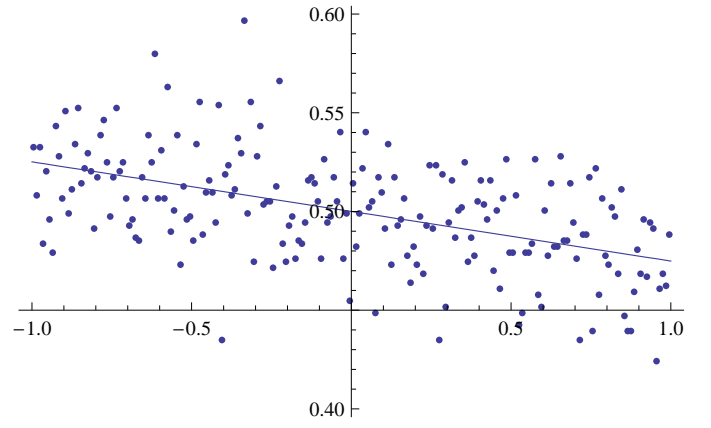


FIG. 12: The fit to the normalized $P(\mu = \hat{L} \cdot \hat{\Delta})$ distribution at $r = 5M$ for $q = 1/4$. The data have been binned with a bin width of $\delta\mu = 0.01$ and normalized to a total probability of 1.

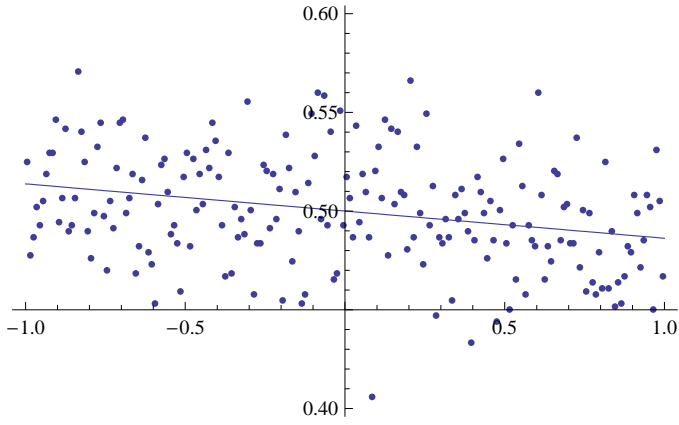


FIG. 10: The fit to the normalized $P(\mu = \hat{L} \cdot \hat{\Delta})$ distribution at $r = 5M$ for $q = 3/4$. The data have been binned with a bin width of $\delta\mu = 0.01$ and normalized to a total probability of 1.

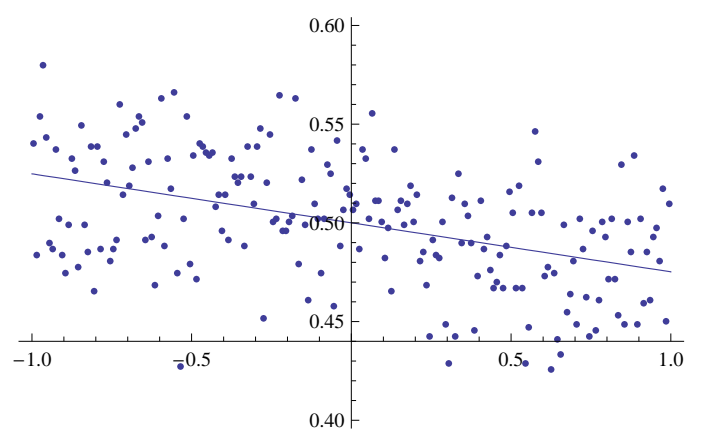


FIG. 13: The fit to the normalized $P(\mu = \hat{L} \cdot \hat{\Delta})$ distribution at $r = 5M$ for $q = 1/8$. The data have been binned with a bin width of $\delta\mu = 0.01$ and normalized to a total probability of 1.

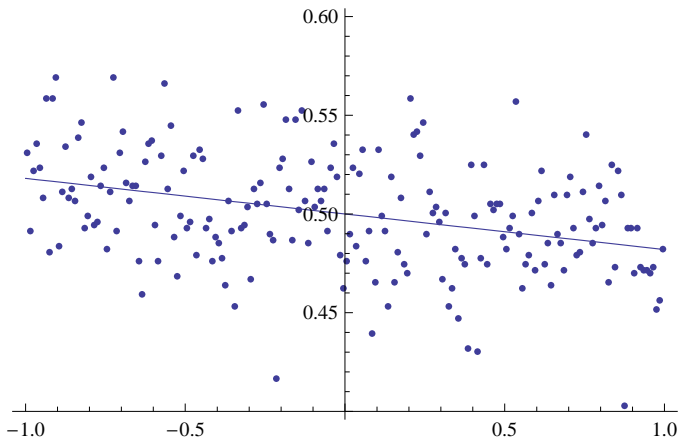


FIG. 11: The fit to the normalized $P(\mu = \hat{L} \cdot \hat{\Delta})$ distribution at $r = 5M$ for $q = 1/2$. The data have been binned with a bin width of $\delta\mu = 0.01$

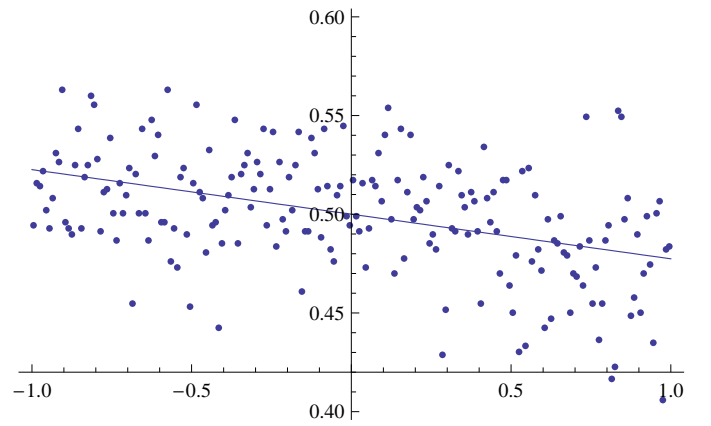


FIG. 14: The fit to the normalized $P(\mu = \hat{L} \cdot \hat{\Delta})$ distribution at $r = 5M$ for $q = 1/16$. The data have been binned with a bin width of $\delta\mu = 0.01$ and normalized to a total probability of 1.

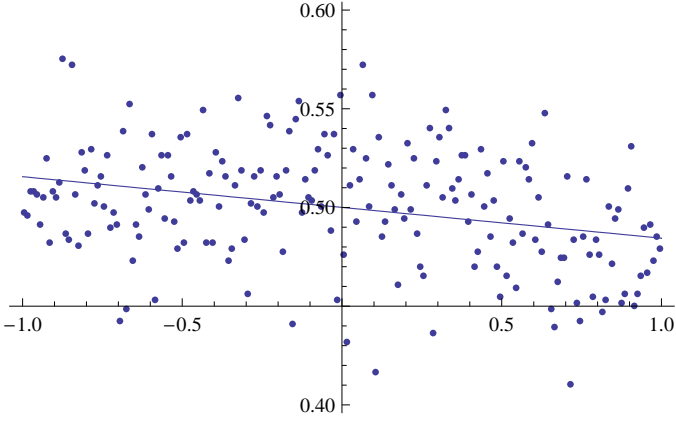


FIG. 15: The fit to the normalized $P(\mu = \hat{\vec{L}} \cdot \hat{\vec{\Delta}})$ distribution at $r = 5M$ for $q = 1/4$ and $\alpha_1 = \alpha_2 = 0.97/\sqrt{2}$. The data have been binned with a bin width of $\delta\mu = 0.01$ and normalized to a total probability of 1.

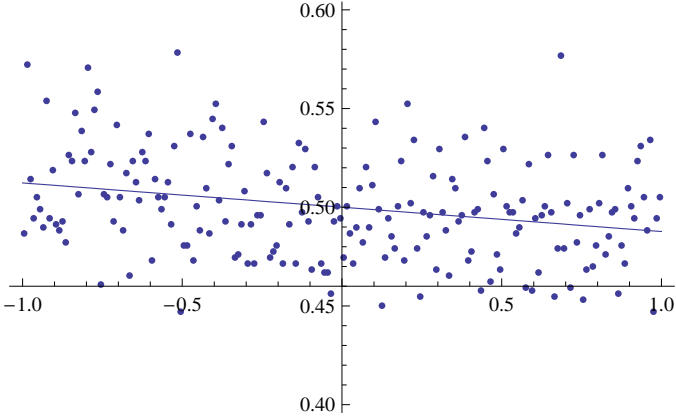


FIG. 16: The fit to the normalized $P(\mu = \hat{\vec{L}} \cdot \hat{\vec{S}})$ distribution at $r = 5M$ for $q = 1/4$ and $\alpha_1 = \alpha_2 = 0.97/2$. The data have been binned with a bin width of $\delta\mu = 0.01$ and normalized to a total probability of 1.

An important consequence of choosing uniform distributions for the directions of \vec{S}_1 and \vec{S}_2 (with magnitude $|\vec{S}_i| = 0.97$) is that the initial distributions for the squares of the magnitudes of \vec{S} and $\vec{\Delta}$, $P(S^2)$ and $P(\Delta^2)$, are uniform in the range $[\alpha(m_2^2 - m_1^2)]^2$ to $[\alpha(m_2^2 + m_1^2)]^2$, and zero outside this range (i.e. there is an equal probability of finding any given value of S^2 or Δ^2 in this range). However the distributions $P(\Delta)$ and $P(S)$ therefore contain an additional linear factor in Δ and S (i.e. $P(x) = 2xP(x^2)$ for any variable x), respectively. One immediate consequence is that the distributions $P(\Delta)$ and $P(S)$ are both maximized for the largest allowed values of S and Δ . Given the observation that large Δ in the orbital plane [7] leads to very large recoils, this bias, if present in nature, would favor observations of large recoils. See Sec. IV for further analysis of the recoil distribution.

Schnittman in Ref. [64] has studied the evolution of

TABLE III: The distribution $P(\mu)$ of the angle $\mu = \cos\theta$ between $\vec{\Delta}$ and the \vec{L} at $r = 5M$ starting from a uniform distribution at $r = 50M$ (top), and the similar distribution for the angle between \vec{S} and \vec{L} (bottom). The 0.25S1 configurations had $\alpha_1 = \alpha_2 = 0.97/\sqrt{2}$ and the 0.25S2 has $\alpha = 0.97/2$, while the 0.25F configurations have $\alpha = 0.97/\sqrt{2}$ and provide the distributions at $r = 8M$ (rather than $r = 5M$), all others had $\alpha_1 = \alpha_2 = 0.97$.

q	$P(\mu)$
1.00	$0.5000 \pm 0.0018 + (0.0009 \pm 0.0031)\mu$
0.75	$0.5000 \pm 0.0019 - (0.0138 \pm 0.0034)\mu$
0.50	$0.5000 \pm 0.0019 - (0.0180 \pm 0.0033)\mu$
0.25	$0.5000 \pm 0.0018 - (0.0251 \pm 0.0031)\mu$
0.125	$0.5000 \pm 0.0020 - (0.0248 \pm 0.0035)\mu$
0.0625	$0.5000 \pm 0.0019 - (0.0226 \pm 0.0033)\mu$
0.25S1	$0.5000 \pm 0.0020 - (0.0156 \pm 0.0035)\mu$
0.25S2	$0.5000 \pm 0.0012 - (0.0123 \pm 0.0031)\mu$
0.25F	$0.5000 \pm 0.0021 - (0.0108 \pm 0.0037)\mu$
1.00	$0.5000 \pm 0.0021 - (0.0345 \pm 0.0037)\mu$
0.75	$0.5000 \pm 0.0020 - (0.0284 \pm 0.0035)\mu$
0.50	$0.5000 \pm 0.0019 - (0.0286 \pm 0.0031)\mu$
0.25	$0.5000 \pm 0.0019 - (0.0261 \pm 0.0034)\mu$
0.125	$0.5000 \pm 0.0018 - (0.0249 \pm 0.0034)\mu$
0.0625	$0.5000 \pm 0.0019 - (0.0225 \pm 0.0033)\mu$
0.25S1	$0.5000 \pm 0.0020 - (0.0162 \pm 0.0034)\mu$
0.25S2	$0.5000 \pm 0.0019 - (0.0125 \pm 0.0034)\mu$
0.25F	$0.5000 \pm 0.0020 - (0.0103 \pm 0.0034)\mu$

TABLE IV: The distribution $P(\mu)$ of the angle $\mu = \cos\theta$ between \vec{S}_1 and the \vec{L} at $r = 5M$ starting from a uniform distribution at $r = 50M$ (top), and the similar distribution for the angle between \vec{S}_2 and \vec{L} (bottom). The 0.25S1 configurations had $\alpha_1 = \alpha_2 = 0.97/\sqrt{2}$ and the 0.25S2 has $\alpha = 0.97/2$, while the 0.25F configurations have $\alpha = 0.97/\sqrt{2}$ and provide the distributions at $r = 8M$ (rather than $r = 5M$), all others had $\alpha_1 = \alpha_2 = 0.97$. Note that the distribution of angles for the smaller component \vec{S}_1 becomes uniform as $q \rightarrow 0$.

q	$P(\mu)$
1.00	$0.5000 \pm 0.0019 - (0.0278 \pm 0.0033)\mu$
0.75	$0.5000 \pm 0.0020 - (0.0129 \pm 0.0034)\mu$
0.50	$0.5000 \pm 0.0019 - (0.0189 \pm 0.0033)\mu$
0.25	$0.5000 \pm 0.0019 - (0.0044 \pm 0.0034)\mu$
0.125	$0.5000 \pm 0.0019 - (0.0000 \pm 0.0033)\mu$
0.0625	$0.5000 \pm 0.0019 - (0.0026 \pm 0.0033)\mu$
0.25S1	$0.5000 \pm 0.0020 - (0.0019 \pm 0.0034)\mu$
0.25S2	$0.5000 \pm 0.0018 - (0.0008 \pm 0.0031)\mu$
0.25F	$0.5000 \pm 0.0021 - (0.0007 \pm 0.0036)\mu$
1.00	$0.5000 \pm 0.0020 - (0.0237 \pm 0.0035)\mu$
0.75	$0.5000 \pm 0.0018 - (0.0252 \pm 0.0032)\mu$
0.50	$0.5000 \pm 0.0020 - (0.0259 \pm 0.0034)\mu$
0.25	$0.5000 \pm 0.0020 - (0.0261 \pm 0.0034)\mu$
0.125	$0.5000 \pm 0.0019 - (0.0249 \pm 0.0034)\mu$
0.0625	$0.5000 \pm 0.0019 - (0.0225 \pm 0.0033)\mu$
0.25S1	$0.5000 \pm 0.0021 - (0.0162 \pm 0.0037)\mu$
0.25S2	$0.5000 \pm 0.0020 - (0.0125 \pm 0.0034)\mu$
0.25F	$0.5000 \pm 0.0020 - (0.0105 \pm 0.0034)\mu$

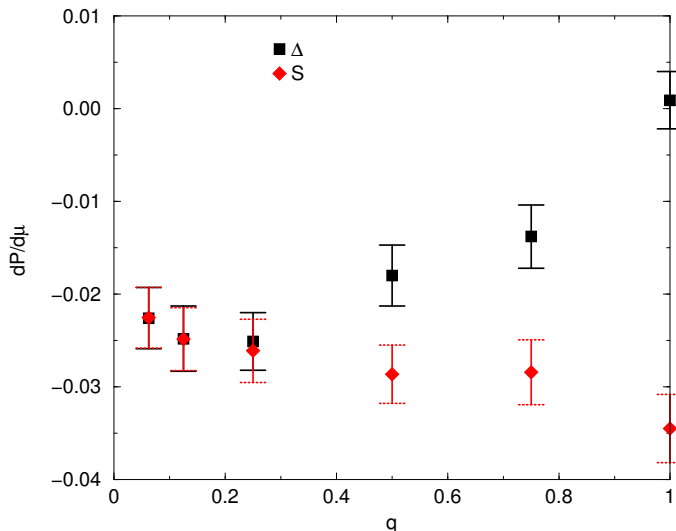


FIG. 17: The dependence of the slope in the distribution of the angle between $\vec{\Delta}$ and the orbital angular momentum, as well as the angle between \vec{S} and the orbital angular momentum as a function of mass ratio.

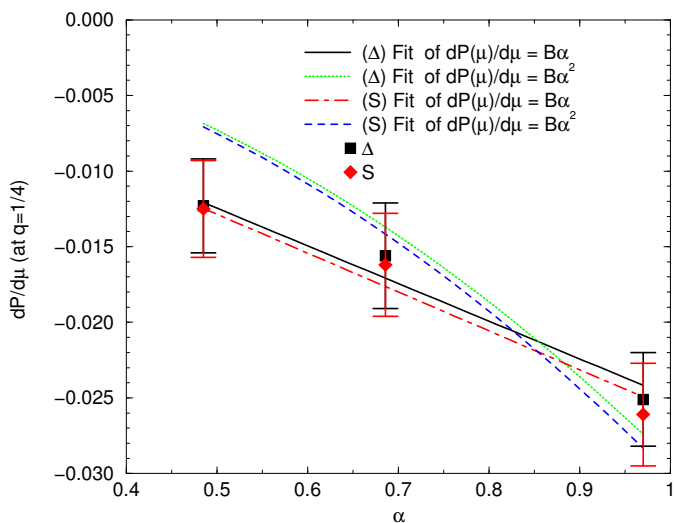


FIG. 18: The dependence of the slope in the distribution of the angle between $\vec{\Delta}$ and the orbital angular momentum \vec{L} for $q = 1/4$ as a function of $|\vec{\alpha}_1| = |\vec{\alpha}_2| = \alpha$, as well as the angle between \vec{S} and the orbital angular momentum as a function of α . In all fits the constant term is taken to be zero. The data here favor a linear dependence in α .

spins in binary systems using orbit-averaged PN equations of motion what allowed longer term evolutions (from separations up to $1000M$). The results indicate strong correlations of the late angle among spins when one starts fixing the initial direction of the spin of the primary object and choose the secondary's spin direction at random (See Figs. 6 and 7 in [64].) Bogdanovic et al revisit this scenario in Ref. [51] and find that if one is allowed to choose initial random distributions for both

spins the resulting evolution leads to close to isotropic distributions of the late directions of the spins (See theirs Fig. 1). In our paper we find an small but statistically significant bias towards counteralignment of the spins with the orbital angular momentum (See Figs. 9-16.)

More recently, Herrmann *et al.* presented numerical studies of the PN equations on GPUs [65]. They used the evolution equation for the orbital frequency assuming quasi-circular orbits. This equation is coupled with the spin and angular momentum precession equations, which include the leading order spin-orbit and spin-spin couplings. On the other hand, in our calculation, the PN equations of motion are derived from the Hamiltonian and include radiation reaction effects. These have higher PN order spin-orbit and spin-spin coupling terms. Furthermore, the second term of the right hand side of Eq. (6) has a significant effect in the PN evolutions. Although the evolution of \hat{L} in [65] is determined only by the conservative dynamics, we have also considered the dissipative effect due to the radiation reaction. We find in the PN prediction that this dissipative effect creates the statistically significant counter-alignment of the spins.

III. MERGER PHASE OF BHBS

Unlike in the earlier inspiral phase, during the plunge and merger the PN equations of motion do not provide a quantitatively accurate description of the merger dynamics, and therefore do not provide robust estimates of the final remnant mass, spin, and recoil. However, analysis of the recoil in particular shows that PN analysis can be used to derive heuristic formulae (based on how PN predictions scale with spins and masses) that give quantitatively correct predictions [7, 24, 66] and incorporate the symmetries of the problem. We will use this modeling in the case of the total radiated energy and angular momentum. In particular we will supplement the inspiral losses, modeled by the energy and angular momentum of the ISCO in the particle limit (extended to the comparable mass regime) with the subsequent plunge using the PN dependence on the BHs parameters (and fitting the amplitudes as in the recoil velocities case).

A. Recoil velocities

In order to quantify and model the nonleading corrections, we augment our original empirical formula with new subleading terms that are higher order in the mass ratio and include a new term linear in the total spin, motivated by higher order post-Newtonian computations[67], and introduce additional parameters

B_H, B_K, H_S, K_S and Θ_1 ,

$$\begin{aligned}
\vec{V}_{\text{recoil}}(q, \vec{\alpha}) &= v_m \hat{e}_1 + v_\perp (\cos \xi \hat{e}_1 + \sin \xi \hat{e}_2) + v_\parallel \hat{n}_\parallel, \\
v_m &= A \frac{\eta^2(1-q)}{(1+q)} [1 + B\eta], \\
v_\perp &= H \frac{\eta^2}{(1+q)} \left[(1 + B_H \eta) (\alpha_2^\parallel - q\alpha_1^\parallel) \right. \\
&\quad \left. + H_S \frac{(1-q)}{(1+q)^2} (\alpha_2^\parallel + q^2\alpha_1^\parallel) \right], \\
v_\parallel &= K \frac{\eta^2}{(1+q)} \left[(1 + B_K \eta) |\alpha_2^\perp - q\alpha_1^\perp| \right. \\
&\quad \times \cos(\Theta_\Delta - \Theta_0) \\
&\quad \left. + K_S \frac{(1-q)}{(1+q)^2} |\alpha_2^\perp + q^2\alpha_1^\perp| \right. \\
&\quad \left. \times \cos(\Theta_S - \Theta_1) \right], \tag{22}
\end{aligned}$$

where $\eta = q/(1+q)^2$, with $q = m_1/m_2$ the mass ratio of the smaller to larger mass hole, $\vec{\alpha}_i = \vec{S}_i/m_i^2$, the index \perp and \parallel refer to perpendicular and parallel to the orbital angular momentum respectively, \hat{e}_1, \hat{e}_2 are orthogonal unit vectors in the orbital plane, and ξ measures the angle between the unequal mass and spin contribution to the recoil velocity in the orbital plane. The constants H_S and K_S can be determined from newly available runs. The angle Θ is defined as the angle between the in-plane component of $\vec{\Delta} = M(\vec{S}_2/m_2 - \vec{S}_1/m_1)$ or $\vec{S} = \vec{S}_1 + \vec{S}_2$ and the infall direction at merger. Phases Θ_0 and Θ_1 depend on the initial separation of the holes for quasircular orbits.

A crucial observation is that the dominant contribution to the recoil is generated near the time of formation of the common horizon of the merging black holes (See, for instance Fig. 6 in [68]). The formula above (22) describing the recoil applies at this moment (more precisely, the coefficients correspond to an averaging of the PN expressions during the plunge phase), and has proven to represent the distribution of velocities with sufficient accuracy for astrophysical applications. The total recoil velocity also acquires a correction [69] for small eccentricities, e , of the form $\vec{V}_e = \vec{V}_{\text{recoil}}(1 + e)$, and if one allows for relativistic close hyperbolic encounters, then recoils up to 10000 km s⁻¹ are possible [70]. Although we expect the orbits will circularize well before merger.

The most recent estimates for the above parameters can be found in [50] and references therein. The current best estimates are: $A = 1.2 \times 10^4$ km s⁻¹, $B = -0.93$, $H = (6.9 \pm 0.5) \times 10^3$ km s⁻¹, $K = (6.0 \pm 0.1) \times 10^4$ km s⁻¹, and $\xi \sim 145^\circ$. Note that we can use the data from [50] to obtain $K = (6.072 \pm 0.065) \times 10^4$ km s⁻¹, if we assume that B_K and K_S are negligible. On the other hand, by fitting the data to K and B_K simultaneously, we obtain $K = (5.24 \pm 0.29) \times 10^4$ km s⁻¹ and $B_K = 0.74 \pm 0.29$. At first glance these two results look quite different. However, in both cases the

actual resulting empirical formula predict the same recoil velocities within 8% over the range $1/10 < q < 1$ (the data from [50] covered the range $1/8 < q < 1$). Finally, if we fit the data to find K and K_S simultaneously we obtain $K = (6.20 \pm 0.12) \times 10^4$ km s⁻¹ and $K_S = -0.056 \pm 0.041$, where we made the additional assumption that since $\vec{S} = \vec{\Delta}$ for these runs, that $\Theta_0 = \Theta_1$. An attempt to fit all three parameters produces inaccurate fitting parameters because the degrees of freedom in the fit and the limited number of available runs.

Equation (22) for the recoil contains all the expected linear terms in the spin, and include ten fitting parameters. Based on the works [67, 71] one could add quadratic terms, but they are complicated expressions with more fitting parameters that we will not include here.

B. Remnant Mass

Motivated by the success of the empirical formula for the recoil, we propose a new empirical formula for the total radiated energy based on the post-Newtonian equations that describe the instantaneous radiated energy (See Eqs. (3.25) in Ref. [46], and for the quadratic terms in the spin see Ref. [67], Eq. (5.6)). For example, the spin-spin contribution to the radiated energy has components quadratic in Δ that have the form,

$$\begin{aligned}
\dot{E}_{SS} &\sim A\Delta^2 + B(\hat{n} \cdot \vec{\Delta})^2 + C(\vec{v} \cdot \vec{\Delta})^2 + D(\hat{n} \cdot \vec{\Delta})(\vec{v} \cdot \vec{\Delta}) \\
&= A(\Delta_\perp^2 + \Delta_\parallel^2) + \Delta_\perp^2 (\tilde{B} \cos^2 \theta + \tilde{C} \cos \theta \sin \theta + \tilde{D}) \\
&= A\Delta_\parallel^2 + b\Delta_\perp^2 (\cos^2(\theta - \theta_0) + c) \\
&= A\Delta_\parallel^2 + \tilde{b}\Delta_\perp^2 (\cos 2(\theta - \theta_0) + \tilde{c}). \tag{23}
\end{aligned}$$

A similar expansion can be derived for the terms quadratic in $\vec{S}_0 = 2\vec{S} + (\delta m/M)\vec{\Delta}$. In addition to the terms arising from the instantaneous radiated energy, that allow for twelve fitting parameters, we also included terms associated with the secular loss of energy in the inspiral period from essentially infinite separation down to the plunge. In order to model this contribution we adopted the form of the the 2PN binding energy, with coefficients chosen to reproduce the particle limit at the ISCO[72]

$$\begin{aligned}
\tilde{E}_{ISCO} &= (1 - \sqrt{8}/3) + \frac{\alpha_2^\parallel}{18\sqrt{3}} \\
&\quad - \frac{5}{324\sqrt{2}} [\vec{\alpha}_2^2 - 3(\alpha_2^\parallel)^2] + \mathcal{O}(\alpha_2^3)
\end{aligned}$$

where we considered terms up to quadratic order in the spin.

If we take into account the η^2 effects from self force calculations [73] and 2PN effects of the spins (See [46],

Eq. (4.6)), we obtain:

$$\begin{aligned}\tilde{E}_{ISCO} = & (1 - \sqrt{8}/3) + 0.103803\eta \\ & + \frac{1}{36\sqrt{3}(1+q)^2} \left[q(1+2q)\alpha_1^\parallel + (2+q)\alpha_2^\parallel \right] \\ & - \frac{5}{324\sqrt{2}(1+q)^2} \left[\tilde{\alpha}_2^2 - 3(\alpha_2^\parallel)^2 \right. \\ & \left. - 2q(\tilde{\alpha}_1 \cdot \tilde{\alpha}_2 - 3\alpha_1^\parallel\alpha_2^\parallel) + q^2(\tilde{\alpha}_1^2 - 3(\alpha_1^\parallel)^2) \right] \\ & + \mathcal{O}(\alpha^3)\end{aligned}\quad (24)$$

This expression represents a quadratic expansion in the spin-dependence, hence we expect to produce reliable results for intrinsic spin magnitudes $\alpha_i < 0.8$. The exact expression for all values of spins, including maximally rotating, are complicated and are given in the appendix

Thus our parametrization of the energy loss is given

$$\begin{aligned}\delta M/M = & \eta \tilde{E}_{ISCO} + E_2\eta^2 + E_3\eta^3 \\ & + \frac{\eta^2}{(1+q)^2} \left\{ E_S (\alpha_2^\parallel + q^2 \alpha_1^\parallel) \right. \\ & + E_\Delta (1-q) (\alpha_2^\parallel - q \alpha_1^\parallel) + E_A |\tilde{\alpha}_2 + q \tilde{\alpha}_1|^2 \\ & + E_B |\alpha_2^\perp + q \alpha_1^\perp|^2 (\cos^2(\Theta_+ - \Theta_2) + E_C) \\ & + E_D |\tilde{\alpha}_2 - q \tilde{\alpha}_1|^2 \\ & \left. + E_E |\alpha_2^\perp - q \alpha_1^\perp|^2 (\cos^2(\Theta_- - \Theta_3) + E_F) \right\},\end{aligned}\quad (25)$$

where $M = m_1 + m_2$ and Θ_\pm are the angles that $\tilde{\Delta}_\pm = M(\tilde{S}_1/m_1 \pm \tilde{S}_2/m_2)$ make with the radial direction during the final plunge and merger (for comparable-mass BHs, a sizable fraction of the radiation is emitted during this final plunge, see for instance Fig. 6 in Ref. [68]). Phases $\Theta_{2,3}$ are parameters that give the angle of maximum radiation for these terms, and depend on the initial separation and parameters of the binary at the beginning of the numerical simulation.

According to the PN theory [74], the leading correction to the radiated energy for small eccentricities has the form $\dot{E} = \dot{E}_C(1 + 157/24e)$, where E_C is the radiated energy in the circular case, which should in principle be added to the above formula. However, it is expected that the orbits will be quite circularized by the time of merger.

To determine the fitting parameters in formula (25) we need to correct some of the numerical data to account for energy already lost by the system in reaching the initial separation of the simulation. That is, some authors choose to normalize their data such that the sum of the horizons masses is 1, which approximates the situation where the energy lost during the prior inspiral is taken into account, while other normalize the initial data to unit ADM mass. In these latter cases, we add the 3PN binding energy of the initial configuration to the calculated radiated energy to obtain an approximation for the total energy radiated by the system in question from infinite separation.

For the non-spinning case we fit the data found in Refs. [75, 76]. Here we fit E_{Rad} versus η , where E_{Rad} is the total radiated energy for a given configuration (where the binding energy is negative). We calculate the binding energy using the 3PN accurate expressions given in [77]. A fit of the resulting data gives $E_2 = 0.341 \pm 0.014$ and $E_3 = 0.522 \pm 0.062$.

For the spinning cases, when spins are aligned with the orbital angular momentum, fits for final remnant mass from Ref. [78, 79] yield $E_S = 0.673 \pm 0.035$, $E_\Delta = -0.36 \pm 0.37$, $E_A = -0.014 \pm 0.021$, and $E_D = 0.26 \pm 0.44$. The source of these large errors is the difference in correcting for the normalization of the results in the papers.

Finally, fits from the final remnant masses from Ref. [24] yields $E_E = 0.09594 \pm 0.00045$ and fits from the equal-mass configurations in Ref. [50] yield $E_B = 0.045 \pm 0.010$.

C. Remnant Spin

In an analogous way, we propose an empirical formula for the final remnant spin (note that the total radiated angular momentum, unlike the total radiated energy, is not finite for an inspiral from infinite initial separation) based on the post-Newtonian equations that describe the radiated angular momentum (See Eqs. (3.28) in [46]) and the angular momentum of a circular binary at close separations (4.7),

$$\begin{aligned}\tilde{\alpha}_{\text{final}} = & (1 - \delta M/M)^{-2} \left\{ \eta \tilde{J}_{ISCO} + (J_2\eta^2 + J_3\eta^3) \hat{n}_\parallel \right. \\ & + \frac{\eta^2}{(1+q)^2} \left(\left[J_A (\alpha_2^\parallel + q^2 \alpha_1^\parallel) \right. \right. \\ & \left. \left. + J_B (1-q) (\alpha_2^\parallel - q \alpha_1^\parallel) \right] \hat{n}_\parallel \right. \\ & \left. + (1-q) |\tilde{\alpha}_2^\perp - q \tilde{\alpha}_1^\perp| \right. \\ & \left. \times \sqrt{J_\Delta \cos[2(\Theta_\Delta - \Theta_4)] + J_{M\Delta} \hat{n}_\perp} \right. \\ & \left. + |\tilde{\alpha}_2^\perp + q^2 \tilde{\alpha}_1^\perp| \right. \\ & \left. \times \sqrt{J_S \cos[2(\Theta_S - \Theta_5)] + J_{MS} \hat{n}_\perp} \right) \left. \right\}.\end{aligned}\quad (26)$$

where we have expanded the triple cross products in Eq. (3.28c) in [46] and used the last form of the parametrization in Eq. (23).

Note that, even at linear order, there are important contributions of generic spinning black holes producing radiation in directions off the orbital axis that do not vanish for equal masses nor vanishing total spin. The above formula can be augmented by quadratic-in-the-spins terms [67, 71] of a form similar to the terms added to the radiated energy formula (25). However, those terms are more complicated and involve many more fitting constants in addition to the ten for the linear dependence. In addition, the linear approximations seem to have smaller quadratic corrections for the radiated angu-

lar momentum than the radiated energy (See for instance Fig. 21 of Ref. [5].)

Looking at the spin expansion of the orbital angular momentum of a particle at the ISCO [72],

$$\begin{aligned} \tilde{J}_{ISCO} = & 2\sqrt{3}\hat{n}^{\parallel} - \frac{4}{9\sqrt{2}} \left[\vec{\alpha}_2 + 2\alpha_2^{\parallel}\hat{n}^{\parallel} \right] \\ & + \frac{2}{9\sqrt{3}} \left[\vec{\alpha}_2^2 - 3(\alpha_2^{\parallel})^2 \right] \hat{n}^{\parallel} + \frac{1}{\eta} \frac{\vec{\alpha}_2}{(1+q)^2} \\ & + \mathcal{O}(\alpha_2^3). \end{aligned} \quad (27)$$

and incorporating the η^2 effects from self force calculations [73] and the 2PN effects of the spins (see Eq(4.7) in [46]), fitted to reproduce the particle limit one obtains,

$$\begin{aligned} \tilde{J}_{ISCO} = & \left\{ 2\sqrt{3} - 1.5255862\eta \right. \\ & - \frac{1}{9\sqrt{2}(1+q)^2} \left[q(7+8q)\alpha_1^{\parallel} + (8+7q)\alpha_2^{\parallel} \right] \\ & + \frac{2}{9\sqrt{3}(1+q)^2} \left[\vec{\alpha}_2^2 - 3(\alpha_2^{\parallel})^2 \right. \\ & \left. \left. - 2q(\vec{\alpha}_1 \cdot \vec{\alpha}_2 - 3\alpha_1^{\parallel}\alpha_2^{\parallel}) + q^2(\vec{\alpha}_1^2 - 3(\alpha_1^{\parallel})^2) \right] \right\} \hat{n}^{\parallel} \\ & - \frac{1}{9\sqrt{2}(1+q)^2} [q(1+4q)\vec{\alpha}_1 + (4+q)\vec{\alpha}_2] \\ & + \frac{1}{\eta} \frac{(\vec{\alpha}_2 + q^2\vec{\alpha}_1)}{(1+q)^2} + \mathcal{O}(\alpha^3). \end{aligned} \quad (28)$$

This expression represents a quadratic expansion in the spin-dependence, hence we expect to produce reliable results for intrinsic spin magnitudes $\alpha_i < 0.8$. The exact expression for all values of spins, including maximally rotating, are complicated and are given in the appendix

According to the PN theory [74], the leading correction to the radiated angular momentum for small eccentricities has the form $J = \tilde{J}_C(1+23/8e)$. This correction can be added to the results, but we expect very low eccentricities by the time the BHs merge (see [80, 81] for the effects of eccentricity on the remnant).

For the non-spinning case we fit the data found in Refs. [75, 76]. We find $J_2 = -2.81 \pm 0.11$ and $J_3 = 1.69 \pm 0.51$. Fits for final remnant spin from Refs. [78] yield $J_A = -1.971 \pm 0.018$, and $J_B = -3.611 \pm 0.042$. The rest of the fitting constants are currently hard to determine with precision. If we attempt to fit J_A and J_B from the data in [78] and [79], we find $J_A = -2.97 \pm 0.26$ and $J_B = -1.73 \pm 0.80$. From the combined fit we find that $2.42\% < \delta M/M < 9.45\%$ and $0.34 < \alpha < 0.92$ for the equal-mass, aligned spin scenario, in the region where the fit is valid ($|\alpha| < 0.9$).

Note that formulae (24) and (28) generalize the particle limit ISCO results to take into account both the mass ratio dependence, $q = m_1/m_2$, and the spin of the holes, S_1 and S_2 , in a symmetric way that is accurate up to quadratic order in those parameters. This allows us to have an accurate description both when the binaries have

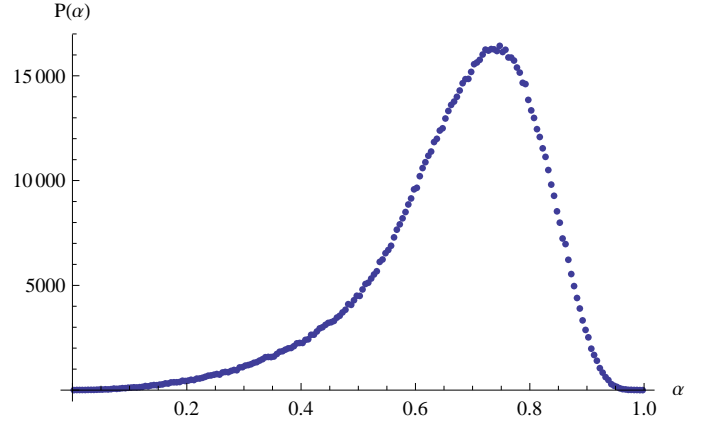


FIG. 19: The remnant BH spin magnitude distribution after several generation of mergers, starting from a uniform initial distribution.

relatively small mass ratios, i.e. $q \lesssim 1/10$, and in the comparable mass regime (where the radiative terms in (25) and (26) dominate and the ISCO is ill defined). For the full expressions see Appendix A.

IV. MERGER STATISTICS

In order to predict the distribution of the remnant spin and recoil, we consider a normal random distribution of spin directions and magnitudes and mass ratios for quasi-circular black-hole binaries and compute the probability density distribution of spin magnitudes of the final remnant (see also [20, 82]). Although our initial PN simulations showed a slight bias towards counter-alignment of the spins to the angular momentum, the effect is small and will be neglected here. The results of ten million of such simulations are displayed in figure 19. The final results are insensitive to the initial distribution and quickly converge, in a few generations of mergers, to the displayed curve, which consequently represents a universal distribution of the intrinsic spin magnitudes [with a maximum near 0.73 and mean in the range (0.53, 0.83)] of remnant BHs (when spin-up effects due accretion are not taken into account). We fit the distribution of the final spins to the Kumaraswamy functional form [83] $f(x; a, b) = abx^{a-1}(1-x^a)^{b-1}$, and find $a = 6.58 \pm 0.08$, $b = 7.14 \pm 0.19$.

Figure 20 show the probability distribution of the magnitude of the final remnant hole's spin for different ranges of the mass ratio q . We observe that the distribution becomes more and more peaked around the value of $\alpha \approx 0.75$ as we go to comparable masses. The distribution gets wider for small mass ratios, this is expected because in the $q \rightarrow 0$ limit one get essentially the original spin distribution of the massive black hole that was taken randomly. Compare this plot with a similar one in Ref. [20], Fig. 1, for dry mergers.

Figure 22 displays the angular dependence of the prob-

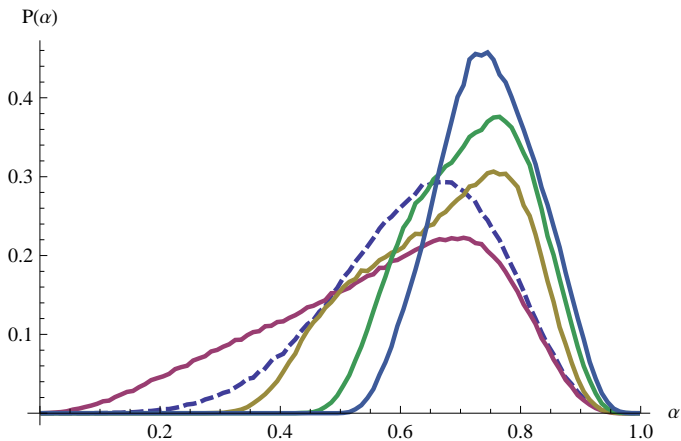


FIG. 20: The remnant BH spin magnitude distribution after several generation of mergers (starting from a uniform initial distribution) for mass ratios in the ranges $0 \leq q \leq 0.1$ (dashed), $0.1 \leq q \leq 0.2$, $0.4 \leq q \leq 0.5$, $0.6 \leq q \leq 0.7$, and $0.9 \leq q \leq 1.0$. The distribution becomes more sharply peaked around larger values of α as the mass ratio increases. Note the for the smallest range, the spin is more highly peaked than for $0.1 \leq q \leq 0.2$.

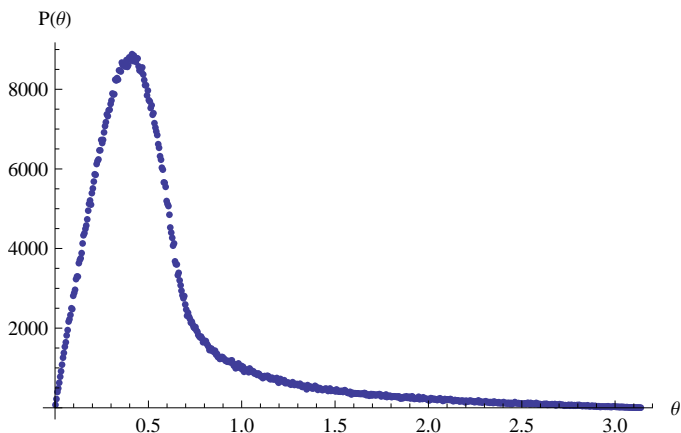


FIG. 21: The remnant spin direction distribution after several generation of mergers, starting from a uniform initial distribution.

ability distribution of the final spin with respect to the original orbital angular momentum at far separations for different ranges of mass ratios. The distribution for comparable masses is peaked at angles close to the orbital angular momentum since the spin contributions tend to cancel leaving most of the contribution to the final angular momentum to the orbital component. We also observe that as we go to smaller mass ratios the distribution becomes wider since the larger black hole contributes randomly to the final total angular momentum. We also observe the vanishing probability of having exact alignment of the final spin with the initial angular momentum. This is because exact alignment is a set of measure zero on the initial random distribution of the spins.

We then use these distributions for the spin-

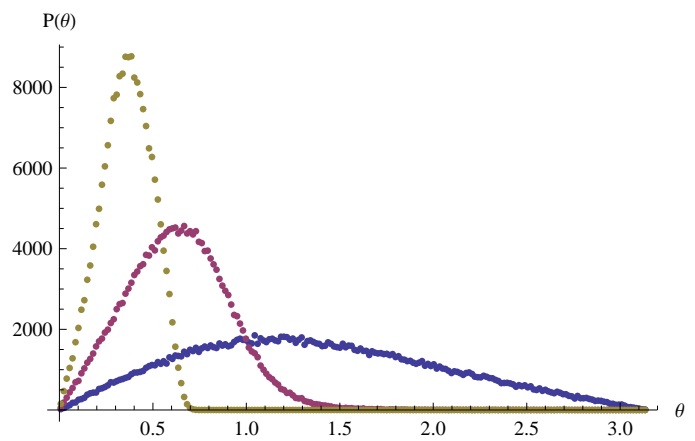


FIG. 22: The remnant spin direction distribution after several generation of mergers, starting from a uniform initial distribution, for mass ratios in the ranges $0 \leq q \leq 0.1$, $0.2 \leq q \leq 0.3$, and $0.9 \leq q \leq 1$. The closer to equal masses, the more highly peaked the distribution. For mass ratios in the range $0.9 \leq q \leq 1$, the distribution is peaked at $\theta \sim 25^\circ$. For the smaller mass ratios, the distribution approaches $\sin \theta$ (i.e. the uniform spin direction distribution).

TABLE V: The probability to obtain large recoil velocities, and large recoil velocities along the line of sight.

$v[\text{km s}^{-1}] \geq$	500	1000	2000	2500
Recoil	50.0%	22.9%	2.11%	0.21%
Observer	22.5%	6.3%	0.21%	0.01%

magnitudes, while assuming uniform distributions in angle and mass ratio, to predict the distribution of recoil velocities. In Figs. 24 and 27 we plot the distribution of recoil magnitudes and directions, respectively. From the plots we see that distribution of recoils in angle is strongly peaked toward alignment and counter-alignment with the orbital angular momentum, which also gives the largest recoil magnitudes (this is a consequence of the fact that the out-of-plane recoil is generally an order magnitude larger than the in-plane recoil, as seen in Eq. (22) and any small component of the spins along the orbital plane lead to those large off-plane recoils.) In Table V we show probabilities for producing various large recoils. In Fig. 23 we plot the distribution of recoil velocities as a function of the angle that the recoil makes with the orbital angular momentum. Here we find that most recoils are aligned (or counter aligned) with the orbital angular momentum (the distributions of recoil velocities $P(v)$ at an angle θ with respect to \hat{L} is identical to the distribution $P(v)$ at an angle $\pi - \theta$). This strong dependence of the magnitude of the recoil with the angle off the orbital plane was to be expected given the large anisotropy found in the empirical recoil formula (22) where the off-orbital plane velocities are an order of magnitude larger than the in-plane ones (i.e. the values of the fitted constants H versus K .)

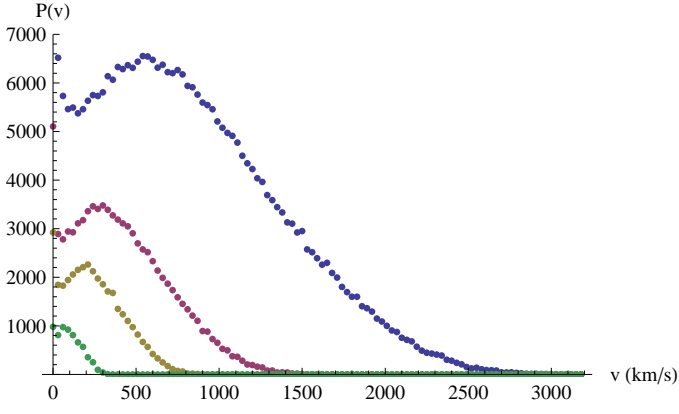


FIG. 23: Velocity distribution as a function of the angle the recoil makes with the orbital angular momentum (the distribution is symmetric with respect to $\theta \rightarrow \pi - \theta$). The plot shows $P(v)$ versus v for recoils with angles in the ranges $(0, 10^\circ)$ (top), $(10^\circ, 20^\circ)$ (2nd), $(20^\circ, 30^\circ)$ (3rd), $(80^\circ, 90^\circ)$ (bottom). The magnitude of $P(v)$ is the total number of simulations with recoil-velocity directions between the given angles and magnitude within the range $v \pm 15 \text{ km s}^{-1}$. The maxima occur at $v(\text{km s}^{-1}) \approx 600, 300, 200, 100$, respectively. These distributions were obtained starting from binaries with a uniform distribution in mass ratio and distribution in spin-magnitude (random directions) given in Fig. 19.

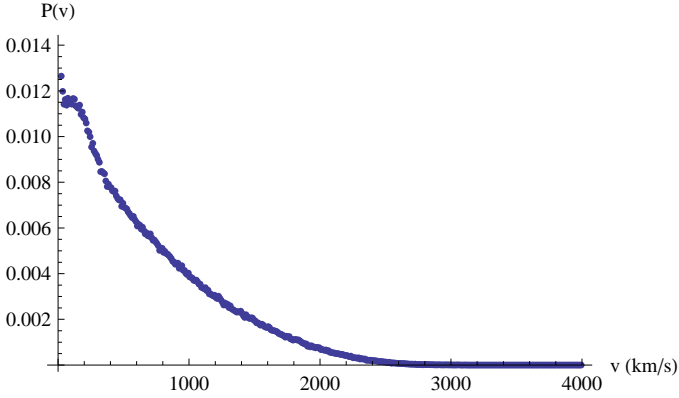


FIG. 24: The recoil velocity magnitude distribution for a uniform distribution in mass ratio and spin-magnitude distribution in Fig 19 (with uniform spin direction). Here $\langle v \rangle = 630 \text{ km s}^{-1}$ and $\sqrt{\langle v^2 \rangle - \langle v \rangle^2} = 534 \text{ km s}^{-1}$.

Figure 26 displays the detailed dependence of the distribution of the magnitude of the recoil velocities with the mass ratio q . Here we observe that for comparable masses we obtain a long tail of large velocity probability which recedes towards smaller velocities as we reduce the mass ratio. This has to do with the suppressing factor η^2 in Eqs. (22). This behavior like q^2 for small mass ratios also explains why the probability shows a peak around $v = 0$. If we consider the probability density function $P(v)$ then $dP = P(v) dv = P(v) \cdot (dv/dq) dq$. Hence $P(v) = (dP/dq)/(dv/dq)$, and since we have chosen a white distribution of q we have $dP/dq = 1$ we obtain

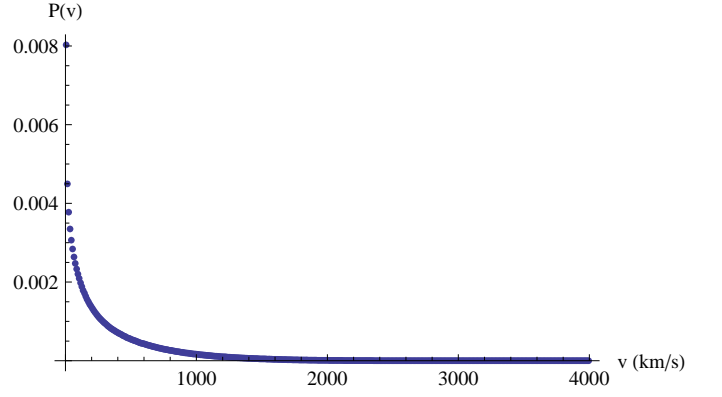


FIG. 25: The distribution of the recoil velocity along an observers line of sight for a uniform distribution in mass ratio and spin-magnitude distribution in Fig 19 (with uniform spin direction). Here $\langle v \rangle = 315 \text{ km s}^{-1}$ and $\sqrt{\langle v^2 \rangle - \langle v \rangle^2} = 358 \text{ km s}^{-1}$.

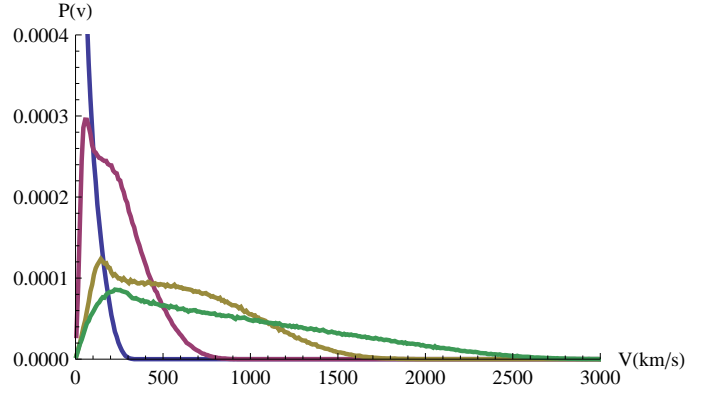


FIG. 26: The recoil velocity magnitude distribution for a uniform distribution in mass ratio and spin-magnitude distribution in Fig 19 (with uniform spin direction). The plot shows the recoil velocity distribution for mass ratios in the range $0 \leq q \leq 0.1$, $0.1 \leq q \leq 0.2$, $0.3 \leq q \leq 0.4$, and $0.9 \leq q \leq 1$. The distributions become successively broader for larger values of q (i.e. similar masses).

$P(v) = 1/(dv/dq) \sim 1/q$, where we have taken the leading dependence from Eq. (22) $v \sim q^2$. This explains the sudden growth of the probability near $v = 0$ when we consider the velocity distribution in the mass ratio range $0 \leq q \leq 0.1$. The wide distributions at intermediate mass ratios has to do with the additional dependence on the direction of the spins of the holes. This distribution drops to near zero again near the maximum recoil velocities $v > 3000 \text{ km s}^{-1}$ since this configurations require not only comparable masses, but also counteralignment of near maximal spins that contribute with a set of measure zero to the total probability density.

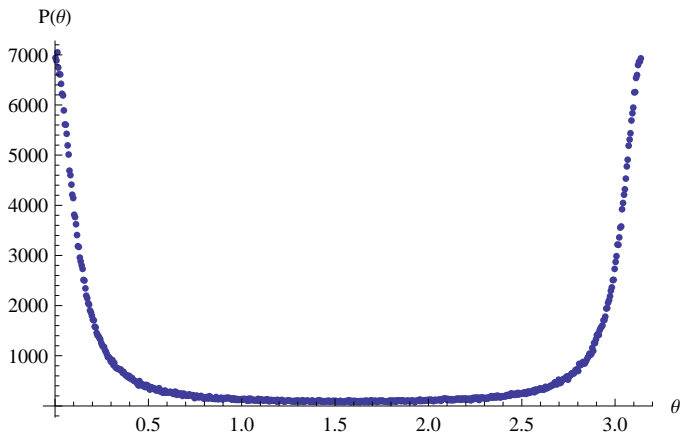


FIG. 27: The recoil velocity direction distribution. The angle θ is in radians, and is defined as the angle between the recoil vector and the orbital angular momentum vector.

V. DISCUSSION

In this paper we studied the ‘dry’ (i.e. gravitational radiation driven) inspiral of black-hole binaries. We performed the evolutions from separations of the order of $50M$, using up to 3.5PN accurate expressions that represents an excellent approximation for this regime (similar simulations with full numerical relativity could prove practically impossible with current technologies). The statistical results show a small bias towards counter-alignment of the vectors $\vec{\Delta}$ and \vec{S} with respect to the orbital angular momentum \vec{L} just prior to merger. This effect essentially takes place at close separations and can be studied analytically at low post-Newtonian orders. The antialignment effect is associated with the late-time precession of the orbital plane due to radiation reaction. This effect for ‘dry’ mergers seems to oppose the alignment mechanism observed in ‘wet’ mergers [51, 52].

After the initial inspiral regime, we studied the merger of black-hole binaries using full numerical simulations. Here we provided a framework to describe the bulk properties of the remnant of a BHB merger based on PN scaling with free parameters fixed by fitting the results of full numerical simulations. We have shown how to determine the mass loss in each BHB encounter (25) and the spin of the remnant BH (26) with fitting constants set to match currently available runs. Using the same methods, one can improve the fitting parameters as the results of new runs are made available, thus providing a standard to incorporate full numerical results into astrophysical applications. The new formulae are physically motivated, as they are derived using the post-Newtonian behavior, and naturally incorporate the correct mass ratio q dependence and physical symmetries, as well as allow for the radiation of angular momentum in the orbital plane. These formulae model the final plunge of comparable masses black holes in an impulsive approximation are supplemented by the slow inspiral losses that precede

this regime by adding the ISCO energy and angular momentum in the particle limit, generalized to symmetric dependence on the mass ratio and spins (Eqs. (24) and (28)).

We also extended the successful recoil formula by adding nonleading terms to include all the linear dependence with the spins, as well as higher mass ratio powers in Eq. (22). Unlike in the formula for the remnant recoil case, the energy and angular momentum lost by the binary during the inspiral phase is a non-trivial fraction of the total radiated energy and angular momentum (and, in fact, is the dominant contribution in the small mass ratio limit). We thus included both the instantaneous radiative terms for the plunge phase as well as the binding energy and angular momentum at the ISCO into our empirical formulae (25) and (26).

Using the fitted coefficients in the above formulae, we find that for equal-mass, non-spinning binaries, the net energy radiated is 5% of the total mass and the final spin is $\alpha \approx 0.69$, both in good agreement with the most accurate full numerical runs [84]. For maximally spinning BHBs with spin aligned and counter-aligned we estimate that quadratic corrections lead to radiated energies between 10% and 3% respectively. As for the magnitude of the remnant spin, the linear estimates are between 0.97 and 0.41 respectively, with quadratic corrections slightly reducing those values. These results show that the cosmic censorship hypothesis is obeyed (i.e. no naked singularities are formed) and are in good agreement with earlier estimates [5].

The set of formulae (25) and (26) with the fitting constants determined as in the Sec. III can be used to describe the final stage of binary black holes mergers in theoretical, N-body, statistical studies in astrophysics and cosmology [51, 82, 85, 86, 87, 88, 89, 90, 91, 92, 93, 94, 95] by choosing a distribution of the initial intrinsic physical parameters of the binaries (q, \vec{S}_1, \vec{S}_2) and mapping them to the final distribution of recoil velocities, spins and masses after the mergers. Here we performed initial studies and have found that: i) The merged black holes have a considerable probability (23%) to reach recoil velocities above 1000 km s^{-1} (See Fig. 24 and Table V) and the distribution is highly peaked along the orbital angular momentum (See Fig. 27). ii) The direction of the spin of the final merged black holes is strongly peaked at an angle of $\approx 25^\circ$ with respect to the orbital angular momentum pre-merger (see Fig. 21), and the spin magnitude is strongly peaked at $S_f/M_f^2 \approx 0.73$ (see Fig. 19). Higher spins are likely if we include the effects of accretion. This information can be useful in modeling the observational effects of supermassive black holes kicked out of their host galaxies [96]. For example, as a first approximation, one may assume that the inner accretion disk is associated with the orbital plane of the merging binary, while the direction of the final spin is associated with the current direction of the radio-jet, and finally that the preferred direction of the kick is along the orbital angular momentum. We can then to reconstruct

3D recoil velocities out of the observer (redshift velocities) information. Also, when modeling the effects of kicks on accretion disks surrounding the merged binary, one should take into account that the most likely recoil velocity depends on the angle with respect to the binary's orbital plane (See Fig. 23).

In order to take into account that one of the main methods to search for recoiling black holes is to look for large differential redshift, typically between narrow band emission lines coming from the host galaxy and broad emission lines from the portion of the accretion disk that the recoiling black hole carries with it [39, 40, 41], we have computed the effect of projecting the computed recoil velocity from the merger of two black holes along the line of sight of an observer on earth. The results are plotted in Fig. 25 and in Table V.

Acknowledgments

We thank E.Bonning, A.Robinson, J. Schnittman, and M.Volonteri for interesting discussions. We gratefully acknowledge NSF for financial support from grant PHY-0722315, PHY-0653303, PHY-0714388, PHY-0722703, DMS-0820923, and PHY-0929114; and NASA for financial support from grant NASA 07-ATFP07-0158 and HST-AR-11763. Computational resources were provided by Ranger cluster at TACC (Teragrid allocations TG-PHY080040N and TG-PHY060027N) and by NewHorizons at RIT.

APPENDIX A: INNERMOST STABLE CIRCULAR ORBIT OF "KERR" GEODESICS

In this appendix we provide the necessary formulae to compute the E_{ISCO} and J_{ISCO} denoted in the empirical equations for the black hole remnant mass and spin, i.e. Eqs. (25) and (26). Note that in the main text we have given explicitly those functions up to quadratic terms in the spin. We also provide explicit analytic expressions of the ISCO radius for equatorial and polar orbits (See Eq. (A21).)

When we treat the spin effects on the equations of motion in the effective one body (EOB) approach, it is

useful to define two combinations of the spins [97], \vec{S}_0 in Eq. (12) and $\vec{\tilde{S}}$,

$$\begin{aligned}\vec{\tilde{S}} &= \vec{S} + \frac{\delta m}{M} \vec{\Delta} \\ &= \frac{m_2}{m_1} \vec{S}_1 + \frac{m_1}{m_2} \vec{S}_2,\end{aligned}\quad (\text{A1})$$

This is because we can rewrite \vec{S} by using the nondimensional spins, $\vec{\alpha}_1$ and $\vec{\alpha}_2$,

$$\vec{\tilde{S}} = m_1 m_2 (\vec{\alpha}_1 + \vec{\alpha}_2), \quad (\text{A2})$$

and then when we consider $\eta = 0$, m_1 or m_2 is zero. We note that this definition of $\vec{\tilde{S}}$ is same as σ in [97] except the numerical coefficient.

Based on the equations given in [98], we focus only on \vec{S}_0 to derive the innermost stable circular orbit (ISCO) of the Kerr spacetime with a spin $a = S_0/M$. Here, we assume that the direction of \vec{S}_0 along the z -axis and we use the Boyer-Lindquist coordinates. In practice, we should use and write "spherical" orbits due to the spins of a binary. But here, we call "circular" orbits.

When we consider the geodesic motion, $z^\alpha(\tau) = \{t_z(\tau), r_z(\tau), \theta_z(\tau), \phi_z(\tau)\}$, where τ is the proper time along the orbit, there are three constants of motion as follows.

$$\begin{aligned}E &= -u^\alpha \xi_\alpha^{(t)}, \\ L_z &= u^\alpha \xi_\alpha^{(\phi)}, \\ Q &= K_{\alpha\beta} u^\alpha u^\beta,\end{aligned}\quad (\text{A3})$$

where $u^\alpha = dz^\alpha/d\tau$, and the two Killing vectors are $\xi_{(t)}^\mu = (\partial_t)^\mu$ and $\xi_{(\phi)}^\mu = (\partial_\phi)^\mu$. And also, we define the Killing tensor, $K_{\mu\nu} = 2\Sigma l_{(\mu} n_{\nu)} + r^2 g_{\mu\nu}$, where $l^\mu = (r^2 + a^2, \Delta, 0, a)/\Delta$ and $n^\mu = (r^2 + a^2, -\Delta, 0, a)/(2\Sigma)$ are two radial null vectors. Here, $\Delta = r^2 - 2Mr + a^2$ and $\Sigma = r^2 + a^2 \cos^2 \theta$. The Killing tensor satisfies the equation $K_{(\mu\nu;\rho)} = 0$. We also define another notation for the Carter constant, $C = Q - (aE - L_z)^2$. For equatorial plane orbits, C defined by this vanishes.

The energy per unit mass for circular orbit with the radius r_{BL} is derived as

$$\begin{aligned}
E = & \left[2Ma (r_{\text{BL}}^2 - 2Mr_{\text{BL}} + a^2) (-r_{\text{BL}}^2 y - r_{\text{BL}}^2 + a^2 y) \right. \\
& \times \sqrt{M(a^4 y + 2r_{\text{BL}}^2 y a^2 - 4Mr_{\text{BL}} y a^2 + r_{\text{BL}}^4 + r_{\text{BL}}^4 y) r_{\text{BL}}^3} \\
& / \left((2y a^4 M r_{\text{BL}} + y a^4 r_{\text{BL}}^2 + y a^4 M^2 + 2y a^2 r_{\text{BL}}^4 - 6y r_{\text{BL}}^2 a^2 M^2 - 4y a^2 M r_{\text{BL}}^3 - 6r_{\text{BL}}^5 M y + r_{\text{BL}}^6 y \right. \\
& \quad \left. + 9M^2 r_{\text{BL}}^4 y - 4a^2 M r_{\text{BL}}^3 - 6r_{\text{BL}}^5 M + r_{\text{BL}}^6 + 9M^2 r_{\text{BL}}^4) (a^4 y + 2r_{\text{BL}}^2 y a^2 + r_{\text{BL}}^4 + r_{\text{BL}}^4 y) \right) \\
& + r_{\text{BL}} (2r_{\text{BL}}^9 y + r_{\text{BL}}^9 y^2 + r_{\text{BL}}^9 + 2r_{\text{BL}}^5 a^4 y + 6r_{\text{BL}}^5 y^2 a^4 + 4r_{\text{BL}}^7 y a^2 + 4r_{\text{BL}}^7 y^2 a^2 + r_{\text{BL}}^8 a^8 y^2 \\
& \quad - 23r_{\text{BL}}^6 M y a^2 - 12r_{\text{BL}}^4 M a^4 y + 33M^2 r_{\text{BL}}^5 y a^2 + 14M^2 r_{\text{BL}}^3 a^4 y - 20r_{\text{BL}}^6 y^2 M a^2 - 18r_{\text{BL}}^4 y^2 M a^4 \\
& \quad + 28M^2 r_{\text{BL}}^5 y^2 a^2 + 8M^2 r_{\text{BL}}^3 y^2 a^4 - 4r_{\text{BL}}^2 y^2 a^6 M - 8M^3 r_{\text{BL}}^4 y a^2 - 4M^3 r_{\text{BL}}^2 a^4 y - 3a^6 M r_{\text{BL}}^2 y \\
& \quad + a^6 M^2 r_{\text{BL}} y - 8M^3 r_{\text{BL}}^4 y^2 a^2 + 4M^3 r_{\text{BL}}^2 y^2 a^4 - 4M^2 r_{\text{BL}} y^2 a^6 - 3r_{\text{BL}}^6 a^2 M - 14r_{\text{BL}}^8 M y \\
& \quad + 5M^2 r_{\text{BL}}^5 a^2 + 32M^2 r_{\text{BL}}^7 y - 7r_{\text{BL}}^8 y^2 M + 16M^2 r_{\text{BL}}^7 y^2 + 4r_{\text{BL}}^3 y^2 a^6 - 24M^3 r_{\text{BL}}^6 y - 12M^3 r_{\text{BL}}^6 y^2 \\
& \quad + a^8 y^2 M - 7r_{\text{BL}}^8 M + 16M^2 r_{\text{BL}}^7 - 12M^3 r_{\text{BL}}^6) / ((2y a^4 M r_{\text{BL}} + y a^4 r_{\text{BL}}^2 + y a^4 M^2 + 2y a^2 r_{\text{BL}}^4 \\
& \quad - 6y r_{\text{BL}}^2 a^2 M^2 - 4y a^2 M r_{\text{BL}}^3 - 6r_{\text{BL}}^5 M y + r_{\text{BL}}^6 y + 9M^2 r_{\text{BL}}^4 y - 4a^2 M r_{\text{BL}}^3 - 6r_{\text{BL}}^5 M \\
& \quad \left. + r_{\text{BL}}^6 + 9M^2 r_{\text{BL}}^4) (a^4 y + 2r_{\text{BL}}^2 y a^2 + r_{\text{BL}}^4 + r_{\text{BL}}^4 y)) \right]^{1/2}. \tag{A4}
\end{aligned}$$

Here, y is introduced as a dimensionless inclination parameter defined by

$$y = \frac{C}{L_z^2}. \tag{A5}$$

This is related to an inclination angle as

$$\begin{aligned}
\cos \iota_{\text{BL}} &= \frac{1}{\sqrt{y+1}} \\
&= \frac{L_z}{\sqrt{C + L_z^2}}, \tag{A6}
\end{aligned}$$

and the inclination angle gives the exact inclination in the case of the Newtonian orbit.

It should be noted that although we can define the circular orbit as a orbit with a constant radius in the

Boyer-Lindquist coordinates, the circular orbit in another coordinates has a time dependent radius [67]. The detail analysis of the gauge transformation have been discussed in [99].

And then, the angular momentum per unit mass along the z-axis is calculated by

$$\begin{aligned}
L_z^2 &= \frac{r_{\text{BL}}^2 (a^2 + 3r_{\text{BL}}^2) E^2}{r_{\text{BL}}^2 y + r_{\text{BL}}^2 - a^2 y} \\
&\quad - \frac{r_{\text{BL}}^2 (3r_{\text{BL}}^2 - 4Mr_{\text{BL}} + a^2)}{r_{\text{BL}}^2 y + r_{\text{BL}}^2 - a^2 y}. \tag{A7}
\end{aligned}$$

Here and hereafter, we focus only on the case that $L_z \geq 0$.

The ISCO radius in the Kerr spacetime is obtained by solving the following equation with respect to r_0 .

$$\begin{aligned}
0 = & (-6r_0^5 M + 4a^2 M r_0^3 - 6a^4 M r_0 + a^6 + 3a^2 r_0^4 + 3a^4 r_0^2 + r_0^6) y^2 \\
& - 2r_0^4 (3a^8 - 12r_0 a^6 M + 8r_0^2 a^6 + 28a^4 M^2 r_0^2 - 60r_0^3 M a^4 + 6a^4 r_0^4 + 24M^2 r_0^4 a^2 \\
& \quad + 28r_0^5 a^2 M - 36M^2 r_0^6 + 12r_0^7 M - r_0^8) y \\
& + r_0^8 (9a^4 - 28a^2 M r_0 - 6r_0^2 a^2 + 36M^2 r_0^2 - 12M r_0^3 + r_0^4). \tag{A8}
\end{aligned}$$

In the following, we discuss the equatorial and polar orbits analytically. In general inclined orbit cases, we need to solve Eq. (A8) numerically.

1. Equatorial circular orbit

For the equatorial orbit, we may consider $y = 0$ in Eq. (A8).

$$\begin{aligned}
0 = & (9a^4 - 28a^2 M r_0 - 6r_0^2 a^2 + 36M^2 r_0^2 \\
& \quad - 12M r_0^3 + r_0^4) \\
& = (3a^2 - r_0^2 + 8\sqrt{M}\sqrt{r_0}a + 6Mr_0) \\
& \quad \times (3a^2 - r_0^2 - 8\sqrt{M}\sqrt{r_0}a + 6Mr_0). \tag{A9}
\end{aligned}$$

This case has been discussed analytically in [100] which we summarize below. It should be noted that we consider the parameter range $-M \leq a \leq M$ and only the orbits with $L_z > 0$ in our treatment.

The appropriate ISCO solution is derived from

$$0 = r_0^2 - 6Mr_0 + 8M^{3/2}\chi\sqrt{r_0} - 3M^2\chi^2, \quad (\text{A10})$$

where $\chi = a/M$. The solution of the above quartic function is obtained as follows. For $\chi > 0$, we have

$$r_{ISCO} = M \left\{ 3 + \sqrt{3\chi^2 + \lambda^2} - \left[(3 - \lambda)(3 + \lambda + 2\sqrt{3\chi^2 + \lambda^2}) \right]^{1/2} \right\}, \quad (\text{A11})$$

and for $\chi < 0$,

$$r_{ISCO} = M \left\{ 3 + \sqrt{3\chi^2 + \lambda^2} + \left[(3 - \lambda)(3 + \lambda + 2\sqrt{3\chi^2 + \lambda^2}) \right]^{1/2} \right\}, \quad (\text{A12})$$

where

$$\lambda = 1 + (1 - \chi^2)^{1/3} \times \left[(1 + \chi)^{1/3} + (1 - \chi)^{1/3} \right]. \quad (\text{A13})$$

We can obtain the well known result, $r_{ISCO} = M$ for $a = M$ and $r_{ISCO} = 9M$ for $a = -M$ from Eqs. (A11) and (A12), respectively.

2. Polar circular orbit

For the polar orbit, we need to consider the limit $y \rightarrow \infty$ in Eq. (A8). This means that we may solve the following equation.

$$0 = (r_0^6 - 6r_0^5M + 3a^2r_0^4 + 4a^2Mr_0^3 + 3a^4r_0^2 - 6a^4Mr_0 + a^6). \quad (\text{A14})$$

Here, we introduce two nondimensional variables, \tilde{r} and χ as

$$\begin{aligned} r_0 &= M\chi\tilde{r}, \\ a &= M\chi. \end{aligned} \quad (\text{A15})$$

Here we consider the case for $\chi \neq 0$. Then, the equation to find the ISCO radius is written as

$$\begin{aligned} 0 &= \tilde{r}^6 - 6\frac{\tilde{r}^5}{\chi} + 3\tilde{r}^4 + 4\frac{\tilde{r}^3}{\chi} \\ &\quad + 3\tilde{r}^2 - 6\frac{\tilde{r}}{\chi} + 1. \end{aligned} \quad (\text{A16})$$

The solutions are nice relations (we can find them from numerical method), and the solutions are given by

$$\begin{aligned} r_s, \frac{1}{r_s}, \exp(i\theta_1), \exp(-i\theta_1), \\ \exp(i\theta_2), \exp(-i\theta_2), \end{aligned} \quad (\text{A17})$$

where r_s, θ_1 and θ_2 are real. The above solutions suggest that the 6th order equation can be reduced to

$$\begin{aligned} 0 &= (\tilde{r}^2 - \alpha_1\tilde{r} + 1)(\tilde{r}^2 - \alpha_2\tilde{r} + 1) \\ &\quad \times (\tilde{r}^2 - \alpha_3\tilde{r} + 1). \end{aligned} \quad (\text{A18})$$

Here, although α_1 is real, α_2 and α_3 are complex and complex conjugate each other. Therefore, we focus on the equation with the real coefficient,

$$0 = (\tilde{r}^2 - \alpha_1\tilde{r} + 1), \quad (\text{A19})$$

where we find

$$\begin{aligned} \alpha_1 &= 2 \frac{\left(1 - \chi^2 + i\chi\sqrt{2 - \chi^2}\right)^{1/3}}{\chi} \\ &\quad + 2 \frac{1}{\chi \left(1 - \chi^2 + i\chi\sqrt{2 - \chi^2}\right)^{1/3}} + 2 \frac{1}{\chi} \\ &= \frac{2}{\chi} (\exp(i\beta/3) + \exp(-i\beta/3) + 1); \\ \tan \beta &= \frac{\chi\sqrt{2 - \chi^2}}{1 - \chi^2}. \end{aligned} \quad (\text{A20})$$

As a result, we have the ISCO radius as the following.

$$\begin{aligned} r_{ISCO} &= M \left\{ \left(1 - \chi^2 + i\chi\sqrt{2 - \chi^2}\right)^{1/3} + \left(1 - \chi^2 + i\chi\sqrt{2 - \chi^2}\right)^{-1/3} + 1 \right. \\ &\quad \left. + \sqrt{\left[\left(1 - \chi^2 + i\chi\sqrt{2 - \chi^2}\right)^{1/3} + \left(1 - \chi^2 + i\chi\sqrt{2 - \chi^2}\right)^{-1/3} + 1\right]^2 - \chi^2} \right\}. \end{aligned} \quad (\text{A21})$$

We show the polar ISCO orbit for the case of $a = 0.9M$

in Fig. 28.

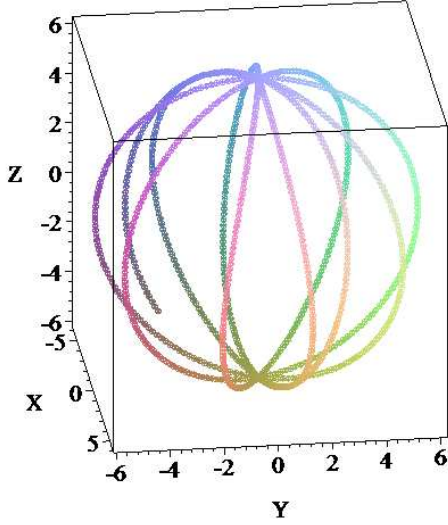


FIG. 28: The polar ISCO orbit in the case of $a = 0.9M$ where we set $M = 1$.

-
- [1] F. Pretorius, Phys. Rev. Lett. **95**, 121101 (2005), gr-qc/0507014.
 - [2] M. Campanelli, C. O. Lousto, P. Marronetti, and Y. Zlochower, Phys. Rev. Lett. **96**, 111101 (2006), gr-qc/0511048.
 - [3] J. G. Baker, J. Centrella, D.-I. Choi, M. Koppitz, and J. van Meter, Phys. Rev. Lett. **96**, 111102 (2006), gr-qc/0511103.
 - [4] M. Campanelli, C. O. Lousto, and Y. Zlochower, Phys. Rev. D **74**, 041501(R) (2006), gr-qc/0604012.
 - [5] M. Campanelli, C. O. Lousto, Y. Zlochower, B. Krishnan, and D. Merritt, Phys. Rev. **D75**, 064030 (2007), gr-qc/0612076.
 - [6] M. Campanelli, C. O. Lousto, and Y. Zlochower, Phys. Rev. D **74**, 084023 (2006), astro-ph/0608275.
 - [7] M. Campanelli, C. O. Lousto, Y. Zlochower, and D. Merritt, Astrophys. J. **659**, L5 (2007), gr-qc/0701164.
 - [8] J. G. Baker et al., Astrophys. J. **668**, 1140 (2007), astro-ph/0702390.
 - [9] F. Herrmann, I. Hinder, D. Shoemaker, P. Laguna, and R. A. Matzner, Astrophys. J. **661**, 430 (2007), gr-qc/0701143.
 - [10] M. Koppitz et al., Phys. Rev. Lett. **99**, 041102 (2007), gr-qc/0701163.
 - [11] J. A. González, M. D. Hannam, U. Sperhake, B. Bruggmann, and S. Husa, Phys. Rev. Lett. **98**, 231101 (2007), gr-qc/0702052.
 - [12] W. Tichy and P. Marronetti, Phys. Rev. **D76**, 061502 (2007), gr-qc/0703075.
 - [13] M. Campanelli, C. O. Lousto, H. Nakano, and Y. Zlochower, Phys. Rev. D **79**, 084010 (2009), 0808.0713.
 - [14] B. Szilagyi, L. Lindblom, and M. A. Scheel (2009), 0909.3557.
 - [15] J. G. Baker, M. Campanelli, C. O. Lousto, and R. Takahashi, Phys. Rev. **D69**, 027505 (2004), astro-ph/0305287.
 - [16] L. Rezzolla et al., Astrophys. J. **679**, 1422 (2008), arXiv:0708.3999 [gr-qc].
 - [17] L. Rezzolla et al., Astrophys. J. **674**, L29 (2008), arXiv:0710.3345 [gr-qc].
 - [18] L. Rezzolla et al., Phys. Rev. **D78**, 044002 (2008), 0712.3541.
 - [19] E. Barausse and L. Rezzolla, Astrophys. J. Lett. **704**, L40 (2009), 0904.2577.
 - [20] W. Tichy and P. Marronetti, Phys. Rev. **D78**, 081501 (2008), 0807.2985.
 - [21] L. Boyle and M. Kesden, Phys. Rev. **D78**, 024017 (2008), 0712.2819.
 - [22] A. Buonanno, L. E. Kidder, and L. Lehner, Phys. Rev. **D77**, 026004 (2008), arXiv:0709.3839 [astro-ph].
 - [23] M. Kesden, Phys. Rev. **D78**, 084030 (2008), 0807.3043.
 - [24] M. Campanelli, C. O. Lousto, Y. Zlochower, and D. Merritt, Phys. Rev. Lett. **98**, 231102 (2007), gr-qc/0702133.
 - [25] Z. Haiman, B. Kocsis, K. Menou, Z. Lippai, and Z. Frei, Class. Quant. Grav. **26**, 094032 (2009), 0811.1920.
 - [26] G. A. Shields and E. W. Bonning (2008), 0802.3873.

- [27] Z. Lippai, Z. Frei, and Z. Haiman (2008), 0801.0739.
- [28] G. A. Shields, E. W. Bonning, and S. Salviander (2007), 0707.3625.
- [29] S. Komossa and D. Merritt, *Astrophys. J.* **683**, L21 (2008), 0807.0223.
- [30] E. W. Bonning, G. A. Shields, and S. Salviander (2007), 0705.4263.
- [31] A. Loeb, *Phys. Rev. Lett.* **99**, 041103 (2007), astro-ph/0703722.
- [32] J. D. Schnittman and J. H. Krolik (2008), 0802.3556.
- [33] B. Devecchi, M. Dotti, E. Rasia, M. Volonteri, and M. Colpi (2008), 0805.2609.
- [34] Y. Fujita, *Astrophys. J.* **691**, 1050 (2009), 0810.1520.
- [35] Y. Fujita (2008), 0808.1726.
- [36] S. Komossa and D. Merritt, *Astrophys. J. Lett.* **689**, 189 (2008), 0811.1037.
- [37] D. Merritt, J. D. Schnittman, and S. Komossa, *Astrophys. J.* **699**, 1690 (2009), 0809.5046.
- [38] M. Volonteri and P. Madau (2008), 0809.4007.
- [39] S. Komossa, H. Zhou, and H. Lu, *Astrophys. J. Letters* **678**, L81 (2008), 0804.4585.
- [40] I. V. Strateva and S. Komossa, *Astrophys. J.* **692**, 443 (2009), 0810.3793.
- [41] G. A. Shields et al. (2009), 0907.3470.
- [42] T. M. Heckman, J. H. Krolik, S. M. Moran, J. Schnittman, and S. Gezari, *Astrophys. J.* **695**, 363 (2009), 0810.1244.
- [43] G. A. Shields, E. W. Bonning, and S. Salviander, *Astrophys. J.* **696**, 1367 (2009), 0810.2563.
- [44] T. Bogdanovic, M. Eracleous, and S. Sigurdsson, *Astrophys. J.* **697**, 288 (2009), 0809.3262.
- [45] M. Dotti et al. (2008), 0809.3446.
- [46] L. E. Kidder, *Phys. Rev. D* **52**, 821 (1995), gr-qc/9506022.
- [47] B. Bruggmann, J. A. Gonzalez, M. Hannam, S. Husa, and U. Sperhake, *Phys. Rev. D* **77**, 124047 (2008), 0707.0135.
- [48] F. Herrmann, I. Hinder, D. M. Shoemaker, P. Laguna, and R. A. Matzner, *Phys. Rev. D* **76**, 084032 (2007), 0706.2541.
- [49] D. Pollney et al., *Phys. Rev. D* **76**, 124002 (2007), 0707.2559.
- [50] C. O. Lousto and Y. Zlochower, *Phys. Rev. D* **79**, 064018 (2009), 0805.0159.
- [51] T. Bogdanovic, C. S. Reynolds, and M. C. Miller (2007), astro-ph/0703054.
- [52] A. Perego, M. Dotti, M. Colpi, and M. Volonteri (2009), 0907.3742.
- [53] M. Dotti et al. (2009), 0910.5729.
- [54] A. Buonanno, Y. Chen, and T. Damour, *Phys. Rev. D* **74**, 104005 (2006), gr-qc/0508067.
- [55] T. Damour, P. Jaranowski, and G. Schafer, *Phys. Rev. D* **77**, 064032 (2008), 0711.1048.
- [56] J. Steinhoff, S. Hergt, and G. Schafer, *Phys. Rev. D* **77**, 081501(R) (2008), 0712.1716.
- [57] J. Steinhoff, S. Hergt, and G. Schafer, *Phys. Rev. D* **78**, 101503 (2008), 0809.2200.
- [58] R. A. Porto and I. Z. Rothstein, *Phys. Rev. Lett.* **97**, 021101 (2006), gr-qc/0604099.
- [59] R. A. Porto and I. Z. Rothstein (2007), 0712.2032.
- [60] R. A. Porto and I. Z. Rothstein, *Phys. Rev. D* **78**, 044012 (2008), 0802.0720.
- [61] R. A. Porto and I. Z. Rothstein, *Phys. Rev. D* **78**, 044013 (2008), 0804.0260.
- [62] K. G. Arun, A. Buonanno, G. Faye, and E. Ochsner, *Phys. Rev. D* **79**, 104023 (2009), 0810.5336.
- [63] K. G. Arun, W. Hikida, H. Nakano, N. Sago, and T. Tanaka, *Prog. Theor. Phys.* **117**, 1041 (2007), gr-qc/0702054.
- [64] J. D. Schnittman, *Phys. Rev. D* **70**, 124020 (2004), astro-ph/0409174.
- [65] F. Herrmann, J. Silberholz, M. Bellone, G. Guerberoff, and M. Tiglio (2009), 0908.3889.
- [66] J. A. González, U. Sperhake, B. Bruggmann, M. Hannam, and S. Husa, *Phys. Rev. Lett.* **98**, 091101 (2007), gr-qc/0610154.
- [67] E. Racine, A. Buonanno, and L. E. Kidder, *Phys. Rev. D* **80**, 044010 (2009), 0812.4413.
- [68] C. O. Lousto and Y. Zlochower, *Phys. Rev. D* **77**, 044028 (2008), 0708.4048.
- [69] C. F. Sopuerta, N. Yunes, and P. Laguna, *Astrophys. J.* **656**, L9 (2007), astro-ph/0611110.
- [70] J. Healy et al., *Phys. Rev. Lett.* **102**, 041101 (2009), 0807.3292.
- [71] C. O. Lousto, H. Nakano, and Y. Zlochower (2008).
- [72] A. Ori and K. S. Thorne, *Phys. Rev. D* **62**, 124022 (2000), gr-qc/0003032.
- [73] L. Barack and N. Sago, *Phys. Rev. Lett.* **102**, 191101 (2009), 0902.0573.
- [74] P. C. Peters, *Phys. Rev.* **136**, B1224 (1964).
- [75] E. Berti et al., *Phys. Rev. D* **76**, 064034 (2007), gr-qc/0703053.
- [76] J. A. Gonzalez, U. Sperhake, and B. Bruggmann, *Phys. Rev. D* **79**, 124006 (2009), 0811.3952.
- [77] L. Blanchet and G. Faye, *Phys. Lett. A* **271**, 58 (2000), gr-qc/0004009.
- [78] E. Berti, V. Cardoso, J. A. Gonzalez, U. Sperhake, and B. Bruggmann, *Class. Quant. Grav.* **25**, 114035 (2008), 0711.1097.
- [79] A. Gopakumar, M. Hannam, S. Husa, and B. Bruggmann, *Phys. Rev. D* **78**, 064026 (2008), 0712.3737.
- [80] U. Sperhake et al., *Phys. Rev. D* **78**, 064069 (2008), 0710.3823.
- [81] I. Hinder, B. Vaishnav, F. Herrmann, D. Shoemaker, and P. Laguna, *Phys. Rev. D* **77**, 081502 (2008), 0710.5167.
- [82] E. Berti and M. Volonteri, *Astrophys. J.* **684**, 822 (2008), 0802.0025.
- [83] M. C. Jones, *Statistical Methodology* **6**, 70 (2009).
- [84] M. A. Scheel et al., *Phys. Rev. D* **79**, 024003 (2009), 0810.1767.
- [85] R. M. O’Leary and A. Loeb (2008), 0809.4262.
- [86] L. Blecha and A. Loeb (2008), 0805.1420.
- [87] M. C. Miller and V. M. Lauburg, *Astrophys. J.* **692**, 917 (2009), 0804.2783.
- [88] D. A. Kornreich and R. V. E. Lovelace (2008), 0802.2058.
- [89] M. Volonteri, F. Haardt, and K. Gültekin (2007), 0710.5770.
- [90] A. Gualandris and D. Merritt (2007), 0708.0771.
- [91] K. Holley-Bockelmann, K. Gültekin, D. Shoemaker, and N. Yunes (2007), 0707.1334.
- [92] J. Guedes et al. (2008), 0812.1216.
- [93] M. Volonteri, G. Lodato, and P. Natarajan, *Mon. Not. R. Astron. Soc.* **383**, 1079 (2008), arXiv:0709.0529.
- [94] J. D. Schnittman, *Astrophys. J. Lett.* **667**, L133 (2007), arXiv:0706.1548.
- [95] J. D. Schnittman and A. Buonanno (2007), astro-

- ph/0702641.
- [96] T. Bogdanovic, M. Eracleous, and S. Sigurdsson (2009), 0909.0516.
 - [97] T. Damour, Phys. Rev. D **64**, 124013 (2001), gr-qc/0103018.
 - [98] N. Sago, T. Tanaka, W. Hikida, K. Ganz, and H. Nakano, Prog. Theor. Phys. **115**, 873 (2006), gr-qc/0511151.
 - [99] S. Hergt and G. Schaefer, Phys. Rev. **D77**, 104001 (2008), 0712.1515.
 - [100] J. M. Bardeen, W. H. Press, and S. A. Teukolsky, Astrophys. J. **178**, 347 (1972).
 - [101] L. Blanchet, A. Buonanno, and G. Faye, Phys. Rev. **D74**, 104034 (2006), gr-qc/0605140.
 - [102] We have used the corrected version of dE/dt in Appendix C of [62]. Instead of Eq. (C11) in [62], we need to use the 2.5PN order spin-orbit coupling effect in Eq. (7.11) of [101] because the spin variables are defined with constant magnitude. In addition, in Eq. (C10) in [62], one should remove the fourth term $\nu\{\cdots\}$ in the expression (K. G. Arun, private communication).